International Journal of Plasticity 165 (2023) 103620

Contents lists available at ScienceDirect

International Journal of Plasticity

journal homepage: www.elsevier.com/locate/ijplas

Atomistically-informed hardening and kinetics models of helium bubble in irradiated tungsten

Changqiu Ji [a], Jianqiao Hu [b], Zhuo Zhuang [a], Yinan Cui [a,*]

[a] Applied Mechanics Laboratory, Department of Engineering Mechanics, School of Aerospace Engineering, Tsinghua University, Beijing 100084, China

[b] State Key Laboratory of Nonlinear Mechanics, Institute of Mechanics, Chinese Academy of Sciences, Beijing, 100190, China

ARTICLE INFO

Keywords:
Helium bubble
Irradiation
Tungsten
Dislocation
Interaction

ABSTRACT

In fusion reactor environment, helium bubble acts as a crucial inducement to the performance degradation of plasma facing tungsten, leading to irradiation hardening and embrittlement. The dislocation interacted with helium bubble directly controls the service reliability and safety of irradiated materials. However, the fundamental question regarding the mechanism and quantitative model of this interaction between dislocation and helium-bubble remains largely unexplored. Based on systematic molecular dynamics studies, the interaction mechanism phase diagram is built as a function of helium bubble characters for different types of dislocations. The atomistically-informed mechanism-based models of irradiation hardening and dislocation-helium bubble reaction kinetics are developed, which consider the climb behavior of edge dislocation, the temperature dependent mobility of screw dislocation, as well as the effects of helium-to-vacancy ratio and size of helium bubble. These models can be directly used in micro and *meso* scale simulations, such as discrete dislocation dynamics and crystal plasticity models. Furthermore, the models well predict the macroscopic experimental results.

1. Introduction

In fusion reactors, the service environment of the first wall material is particularly harsh, which is subjected to neutron irradiation, mechanical and thermal conditions (Zinkle and Busby, 2009). In particular, deuterium-tritium fusion reactions produce abundant helium (He) atoms, which have extremely low solubility in metallic materials (Xie et al., 2018). With the high mobility of helium interstitials and the strong tendency of binding between helium and vacancies, helium is deeply trapped in vacancies, decreasing the mobility of vacancies and enhancing the accumulation of additional vacancies and helium atoms (Trinkaus and Singh, 2003). It tends to accumulate and agglomerate to form populous nanometric He-filled bubbles in irradiated materials. Nanoscale helium bubbles lead to surface erosion, such as fuzz and flake formation (Gao and Ghoniem, 2018; Wang et al., 2021b). The formation of a high density of subsurface bubbles drastically deteriorates the mechanical properties of metals, manifested as swelling, blistering, embrittlement, loss of ductility, and reduction of thermal conductivity, etc.

The fundamental scientific problem of dislocation-helium bubble interaction directly controls the service reliability and safety of irradiated materials. On the one hand, helium bubbles obstruct dislocation motion, leading to irradiation hardening. On the other hand, they may be swept away, absorbed, or destroyed by moving dislocations, causing the formation of defect-free channels (so-called

* Corresponding author.
E-mail address: cyn@mail.tsinghua.edu.cn (Y. Cui).

https://doi.org/10.1016/j.ijplas.2023.103620
Received 8 February 2023; Received in revised form 4 April 2023;
Available online 28 April 2023
0749-6419/© 2023 Elsevier Ltd. All rights reserved.

dislocation channels or cleared channels) and the appearance of deformation localization (i.e. micro shear band), which is a primary origin of irradiation embrittlement and stress corrosion cracking. The phenomena of dislocation channel formation and strain localization are widely observed in irradiation materials containing helium bubbles (Ding et al., 2016; Beck et al., 2017; Das et al., 2018; Das et al., 2019). However, how to quantitatively describe the effect of helium bubble on the macro and micro mechanical performance of irradiated material is far from well understood. Tungsten is one of the most promising candidates for plasma facing materials in the International Thermonuclear Experimental Reactor (ITER) and demonstration power plant (DEMO), due to its favorable physical properties, such as high melting temperature, high thermal conductivity, low sputtering yield, and near zero tritium retention (Hirai et al., 2014; Chen et al., 2018; Das et al., 2020). Therefore, a systematic study is required for helium bubble effect in tungsten. Several unresolved questions are listed as follows.

Firstly, the helium bubble itself has particularity and complexity. The number of helium atoms with respect to the number of vacancies, namely the He/V ratio, is a main character involved in helium bubble. It is found that He/V ratio varies with the irradiation temperature, rates of atomic displacements and He generation (Osetsky and Stoller, 2015). There is an equilibrium range of He/V in the helium bubble. Bubbles with a higher He/V ratio are over-pressured and mechanically unstable. For tungsten, the equilibrium He/V ratio mainly falls in 2∼4 from previous studies (Faney, 2013; Li et al., 2014; Yi et al., 2017; Hammond et al., 2018; Zhan et al., 2019). There are mainly three mechanisms keeping He/V below the equilibrium ratio. If there are not enough vacancies available in the material, the mobile pure He cluster separates vacancy from the lattice and be trapped by the vacancy created by itself as its binding energy with the vacancy is quite large (Gao and Ghoniem, 2018), and this is the self-trapping (also called kick-out) mechanism. If one or more vacancies are already trapped inside the He cluster, it can further absorb vacancy or vacancy clusters from the lattice through the trap mutation or loop punching mechanism (Boisse et al., 2014; Wang et al., 2015). In addition, if there is edge dislocation near the helium bubble with high internal pressure, it has been found that the dislocation climb mechanism is shown to be more energetically favorable than the loop punching mechanism for bubble growth. In this way, the bubble absorbs the vacancies from the edge dislocation, accompanied with the climb of dislocation (Xie et al., 2018). Therefore, the first aim of this work is to investigate the influence of He/V ratio on dislocation-helium bubble interaction within or slightly beyond the stable range of He/V.

Secondly, how the interaction with dislocation influences the kinetics of helium bubble is unknown. Till now, the fundamental studies regarding dislocation-helium bubble interaction in tungsten are very limited. Due to lack of systematic studies, their interaction process can only be inferred from the studies on dislocation-void interactions, which is still a matter of debate. Previous work revealed that voids lost the outermost vacancies on the compressive glide plane of the edge dislocation during dislocation-void interaction, making the void shrink or even get damaged in iron (Osetsky and Bacon, 2003b; Tehranchi et al., 2017; Ji et al., 2022). However, for tungsten, Liu et al. (2004) found that the small void does not shrink after being bypassed by an edge dislocation but large void does. A recent study (Yu et al., 2022) also claimed that voids lose vacancies and decrease in size after the reaction with dislocations. Osetsky (2021) disclosed that after interaction with void, the edge dislocation's extra half plane expands, indicating that the void absorbs vacancies and expands in size, which is different from the previous understanding of various materials such as iron (Osetsky and Bacon, 2003b), molybdenum (Dutta et al., 2012), and tungsten (Liu et al., 2004). Therefore, clarifying the mystery why different dislocation-void interaction behaviors are observed, and further developing a dislocation-helium bubble interaction model is the second aim of the current work.

Thirdly, there is a lack of systematic research on helium bubble hardening induced by the block effect of helium bubbles on dislocation movement. Only a few studies on the interaction between edge dislocations and voids in tungsten (Liu et al., 2004; Osetsky, 2021; Yu et al., 2022) are available now. Simulation about edge dislocation-void interactions using Green's function boundary relaxation (Liu et al., 2004) found that the strength of tungsten is consistent with that predicted from the Russell and Brown (R&B) model, which is initially presented for calculating the strength of a precipitation-hardening system containing attractive obstacles (Russell and Brown, 1972). Recently, Osetsky (2021) and Yu et al. (2022) both investigated the interaction between edge dislocations and a periodic array of voids in tungsten, and concluded that the Bacon–Kocks–Scattergood (BKS) hardening model well describes void hardening in tungsten. Nevertheless, how to extend the model of void hardening to helium bubble hardening is unclear yet. On the other hand, previous studies have mostly focused on the interaction between irradiation defects and edge dislocations. Screw dislocations in body centered cubic (BCC) metals have non-planar core structures with strong temperature dependence, which dominate plastic deformation of BCC material at low and medium temperatures, but the interaction between screw dislocations and irradiation defects in BCC metals has been rarely studied. Furthermore, lots of dislocations are mixed in type, but the understanding of its interaction with irradiation defects is even more limited. There is no systematic study or hardening model on the interaction between different types of dislocations and helium bubbles in tungsten till now. Therefore, how to establish a unified framework for describing the hardening results of helium bubbles interacting with different types of dislocations is the third key question to be solved in this work. Considering that the first wall material of fusion reactor experiences a wide range of temperatures during its services, such as the initial heating stage, the subsequent high heat flux and cooling stage, the further aim of the developed model is being able to consider the temperature dependent feature of tungsten plasticity, so as to enhance its prediction capability.

To achieve the goals discussed above, systematic molecular dynamics (MD) studies are carried out to study the interaction between dislocations and helium bubbles. This paper is organized as follows: the simulation schemes are presented in Section 2. Section 3 aims to give a basic understanding of interaction between the edge/screw dislocation and helium bubble in tungsten. In Section 4, a kinetics model of helium bubbles is proposed. Section 5 is denoted to analyze the hardening effect to build a comprehensive hardening model and a yield strength model incorporating helium bubbles. Some applications of the proposed model in multiscale simulations and predicting experiments are discussed in Section 6. Finally, conclusions are summed up in Section 7.

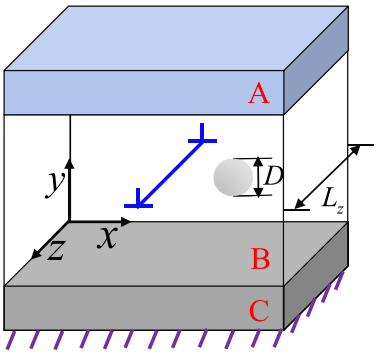

Fig. 1. Schematic of the simulation cell containing the dislocation and helium bubble with diameter D. The dislocation lies along the z direction, and the length of the box in z direction is L_z. Thus helium bubble spacing is $L = L_z - D$. The regions A, B and C contain static atoms to control the deformation of the system, mobile atoms and static atoms to anchor the sample, respectively.

2. Simulation setup

The MD calculations are performed utilizing the Large-scale Atomic/Molecular Massively Parallel Simulator (LAMMPS) software package (Plimpton, 1995). W-W, W-He and He-He interatomic interactions are described by embedded atom method (EAM) (Daw and Baskes, 1984) interatomic potential[1] provided by Bonny et al. (2014). This potential is based on the interatomic potential for W-W interaction developed by (Marinica et al., 2013) and is created aiming at investigating the interaction of H and He with dislocations in tungsten (Grigorev et al., 2018). The detailed validation of the potential including point defect properties, binding energy between atom pairs, binding energy of various clusters, etc., can be found in Bonny et al. (2014). This potential provides a helium migration barrier which agree with the density function theory (DFT) result (Ye et al., 2020; Wang et al., 2021a), and was successfully applied in extensive MD studies of helium bubble formation (Hamid et al., 2019; Ye et al., 2020), migration (Wang et al., 2021a), burst (Zhang et al., 2022) and its effect on thermal conductivity (Zhang et al., 2020) in tungsten.

As schematically shown in Fig. 1, the considered box cell is 41.3 nm × 22.4 nm × 41.5 nm and contains about 2.5 million atoms. A dislocation with line direction along *z* axis and normal direction of the slip plane along *y* axis is introduced into the system using the ATOMSK software package (Hirel, 2015), followed by energy minimization using the conjugate gradient relaxation method. Helium bubbles are constructed by removing all atoms in a spherical region whose center is on the glide plane of dislocation in the sample, and adding a certain number of helium atoms in the sphere randomly. After the helium bubble is inserted, energy minimization is carried out again to relax the system and obtain the initial static equilibrium. Subsequently, with vacuum regions above the top surface and below the bottom surface, the isobaric-isothermal (NPT) ensemble is applied to the system for thermal equilibration, and after that, vacuum regions are deleted (Jian et al., 2020).

Periodic boundary conditions are imposed along the *x* and *z* axis directions. Therefore, the model actually simulates the interaction of a periodic array of infinitely long dislocations along the *z* direction and an array of helium bubbles in a slab of finite thickness (Yu et al., 2022). Atoms in the upper region A are constrained to remain static and control the deformation of the system. Region C contains static atoms and is used to anchor the sample to avoid its drift along the direction of the applied strain. Both atoms in regions A and C have a speed and acceleration remaining at zero. Atoms in region B move following Newton's equation based on the simulation ensemble. The dislocation interacts with helium bubble in this region. This kind of boundary condition is commonly used for molecular dynamics simulation of dislocation-irradiation defect interaction, and proven to be reliable by a large number of previous results (Osetsky and Bacon, 2003a; Hafez Haghighat and Schäublin, 2010; Jian et al., 2020; Yu et al., 2022).

Shear strain loading mode is applied in the simulation. The strain increment adopted is $\Delta\varepsilon = 1 \times 10^{-5}$. After each incremental step, atoms in region B are relaxed by 1 ps with the Nosé-Hoover thermostat employed to maintain the temperature. Therefore, the corresponding strain rate is $1 \times 10^{7}/s$ in this study, which is found to be reasonable, as discussed in Appendix A. Visualization and analysis of the atomic structures and crystal defects are implemented in Open Visualization Tool (OVITO) program (Stukowski, 2010).

The fundamental behavior of edge dislocation and screw dislocation in BCC tungsten is significantly different. Their interactions with helium bubbles are also expected to be different. Therefore, both edge and screw dislocations are considered in the current work. For edge dislocation-helium bubble interaction simulation, the *x, y* and *z* axes of the simulation crystal are oriented along the [111], $[\bar{1}10]$ and $[\bar{1}\bar{1}2]$ directions, respectively. The edge dislocation with the slip direction along *x* and Burgers vector $\mathbf{b} = a/2 < 111 >$ is introduced with the method provided by Osetsky and Bacon (2003a), where *a* is the lattice constant as 3.14 Å (Bonny et al., 2014). Rigid displacement increment is applied in the *x* direction to atoms in the upper region A. The component of applied strain is ε_{xy}, and atomistic shear stress is calculated as the averaged σ_{xy} component over atoms in region B.

The core structure of edge dislocation is planar while the screw dislocation is non-planar and decomposed on three sides in BCC tungsten (Vítek et al., 1970). Therefore, the slip resistance of screw dislocation is prominently higher than that of edge dislocation, and

[1] "EAM2" version as stated in the original paper

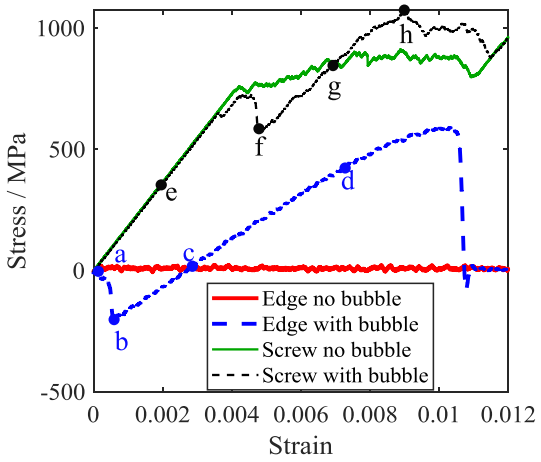

Fig. 2. Stress-strain curves of the box cell containing edge or screw dislocation without and with helium bubble. Marked points (a-d) and (e-h) correspond to the configurations shown in Fig. 3 (a-d) and Fig. 4 (a-d), respectively.

it is difficult to glide. The constriction and spreading of the dislocation core may be influenced by non-glide stress components, leading to non-Schmid effects (Tian and Woo, 2004; Butler et al., 2018). To simulate screw dislocation bypassing helium bubble, the crystallographic directions parallel to the *x*-, *y*- and *z*-axes are $[\bar{1}\bar{1}2]$, $[\bar{1}10]$ and $[111]$, respectively. The component of the applied strain is ε_{yz}, and the atomistic shear stress is calculated as the averaged σ_{yz} component over atoms in region B. Instead of applying traditional periodic boundary, shifted periodic boundary condition is applied along the *x* direction by shifting atomic positions by $\pm b/2$ along the *z* direction to ensure the continuity of the {111} planes across the boundary, following the method proposed by Rodney (Rodney, 2004).

Most of the simulations are carried out at a temperature of $T = 300$ K in this study because the majority of experimental mechanical testing is performed at room temperature (Osetsky and Stoller, 2015). To understand the temeprature effect, other temperatures ranging from 100 K to 900 K are also investigated.

The range of He/V ratio of the considered helium bubbles is from 0 to 5, which not only covers mechanically stable helium bubbles under relevant experimental conditions, but also includes the void case and a few high He/V ratio cases to demonstrate the dramatic change in the interaction mechanism due to over-pressurized conditions. Usually, void and helium bubble are collectively referred to as cavity. Note that void is also described by helium bubble with the ratio $\mathrm{He}/V = 0$ for the convenience of description in this study.

The helium bubble sizes of interest are mainly in the range of 1 to 5 nm, which covers experimental helium bubble sizes in bulk tungsten (Nishijima et al., 2004; Harrison et al., 2017; Kong et al., 2017; Ipatova et al., 2021), and larger helium bubbles have also been briefly investigated. Since helium atoms are much smaller than tungsten atoms, the size of helium bubble is considered to be only dependent on the number of vacancies in it. Therefore, He/V ratio has little effect on the size of helium bubble, and mainly influences its internal pressure.

3. Dislocation-helium bubble interaction mechanism

In this section, the physical process of the edge and screw dislocations interacting with helium bubbles in tungsten are analyzed. The influence of He/V ratio and size of helium bubble is investigated, and phase diagrams for the interaction mechanism are given.

3.1. Interaction process

A basic physical scenario of the dislocation-helium bubble interaction in tungsten is given here. Firstly, the glide behavior and the mechanical response of edge and screw dislocation without helium bubble is studied for comparison purpose. Then, the interaction process and the mechanical behavior of edge and screw dislocations interacting with helium bubble is discussed. The size of helium bubble is taken to be 5 nm and He/V is set to 2 as an example here. The effect of He/V ratio and bubble size is further discussed in Sections 3.2 and 3.3, respectively.

For both edge and screw dislocations gliding under shear without bubble at 300 K, the stress firstly rises with a slope equal to the shear modulus until the stress is large enough to overcome the lattice resistance, as shown in Fig. 2. Then the dislocation moves smoothly with an almost stable stress. As a result of the three-dimensional dislocation core structure, the critical resolved shear stress (CRSS) for the glide of screw dislocation is very high, close to 760 MPa, while the edge dislocation can glide at a CRSS of about 9 MPa. In addition, the edge dislocation keeps straight and glides along the original [111] slip direction. Nevertheless, screw dislocations keep changing slip planes through cross slip, causing the trajectories of points on screw dislocation to be not straight, but a combination of segments $[\bar{1}10]$, $[\bar{1}01]$ and $[0\bar{1}1]$, similar to the previous work of screw dislocation movement under shear in tungsten (Tian and Woo, 2004). The overall glide direction of the screw dislocation is mainly along the *x* axis (the glide direction according to the peach-koehler

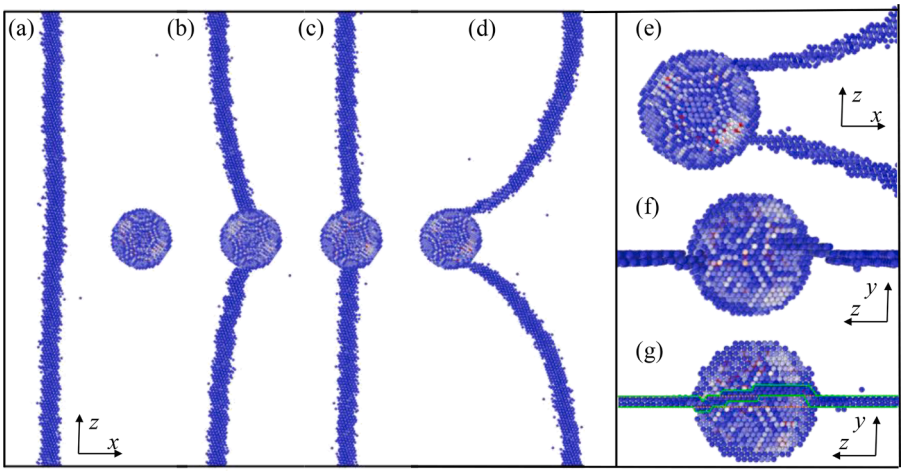

Fig. 3. (a-d) Interaction process of an edge dislocation and a 5 nm helium bubble whose He/V is 2. (e) Screw-like diploe during pinning. (f) Other view of the microstructure configuration corresponds to (e), showing dislocation climb on the bubble surface. (g) Edge dislocation and helium bubble after interaction, with the climbed dislocation configuration underlined by the green line and the initial dislocation configuration underlined by the orange dashed line.

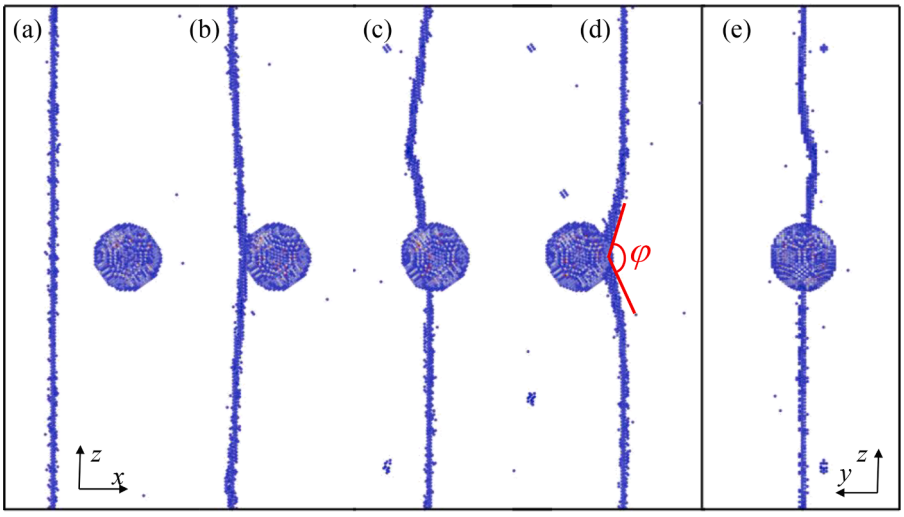

Fig. 4. (a-d) Interaction process of screw dislocation and a 5 nm bubble whose He/V is 2. (e) Curved dislocation line induced by cross slip, as other view of the state of (c).

force) and slightly biased to the *y* direction. The stress fluctuation is also expected to be associated with the cross slip behavior.

When the helium bubble is considered, the maximum stress value is higher than that without helium bubble, indicating the irradiation hardening behavior. There are common features for the interaction process of edge and screw dislocation and helium bubble. Marked points (a-d) and (e-h) in Fig. 2 correspond to the snapshots of the microstructures shown in Fig. 3(a-d) and Fig. 4(a-d), respectively. With the existence of helium bubble, both edge and screw dislocations initially keep straight, and the shear stress keeps increasing until the dislocation starts to glide, as shown in Figs. 3(a) and 4(a). As it moves close to the helium bubble, the middle part of the dislocation line is attracted by the bubble, accompanied with the decrease of stress, corresponding to point b and f in Fig. 2. Then the dislocation at both ends continues to move forward, making the dislocation straight again (see Figs. 3(c) and 4(c)). Subsequently, both ends of the dislocation continue to move forward and bow out, while its middle part is pinned by the bubble, as displayed in Figs. 3(d) and 4(d), and the stress increases continuously during this process. As the shear stress reaches the CRSS for depinning, the dislocation breaks away, and depinning occurs. Afterwards, the stress decreases to the level of that without bubble.

In the following, more details about the depinning mechanisms of the edge and screw dislocation-helium bubble interaction are analyzed, respectively.

The interaction process between edge dislocation and the 5 nm and $He/V = 2$ helium bubble is found to be similar to the interaction between edge dislocation and void in previous work of tungsten (Liu et al., 2004; Osetsky, 2021; Yu et al., 2022). During pinning,

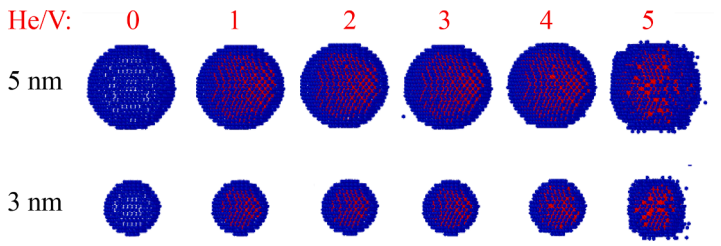

Fig. 5. Helium bubble configuration for helium-to-vacancy ratio ranging from 0 to 5 and diameter of 5 nm and 3 nm. Tungsten atoms on the outer surface of the helium bubble are colored blue and helium atoms inside are red.

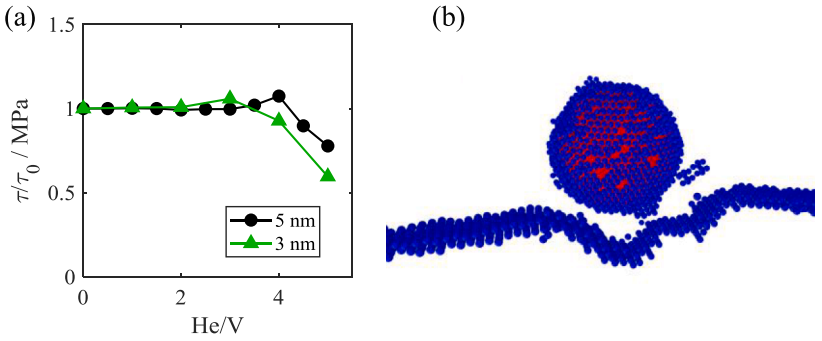

Fig. 6. (a) The normalized CRSS of edge dislocation interacting with helium bubble with diameter of 3 nm and 5 nm and varied He/V ratios. τ_0 for 5 nm and 3 nm helium bubbles are 594 MPa and 480 MPa, respectively. (b) Climbed dislocation after interacting with a 5 nm helium bubble with He/$V = 5$.

dislocation arms are dragged to form a screw-like dipole near the bubble, as shown in Fig. 3(e). Dislocation climbs on the bubble surface and forms super jogs during interaction, as displayed in Fig. 3(f). As a result of climb, a small segment of the edge dislocation leaves its glide plane and dislocation configuration changes. The dislocation and bubble after the reaction are shown in Fig. 3(g), with the climbed dislocation configuration underlined by the green line and its initial configuration underlined by the orange dashed line. This suggests that the climb-assisted glide is the dominant unpinning mechanism for edge dislocation interacting with a 5 nm bubble whose He/V is 2.

For screw dislocation interacting with the helium bubble, Fig. 4(e) gives the snapshots of the microstructure configuration with the view angle perpendicular to the slip plane, which shows that the screw dislocation leaves its original slip plane and cross slip during the interaction. With the assistance of cross slip, screw dislocation easily passes through the helium bubble. The detachment angle φ (marked in Fig. 4(d)) appears to be higher than 90°, suggesting that the bubble does not provide a very strong obstacle against screw dislocation motion, and the hardening stress is lower compared to that of edge dislocation. After bypassing the bubble, screw dislocation returns to its original glide plane, leaving small loops or debris inside the sample. The cross slip assisted depinning mechanism is also observed in prior experiments of BCC materials (Tougou et al., 2022).

Based on the above pinning-depinning process of both edge and screw dislocation interacting with helium bubble, the hardening stress is related to the two common characteristic lengths, namely, the helium bubble size and helium bubble spacing (i.e., the distance between two pinning points of dislocation). Edge dislocation climb hardly affects the characteristic length of interaction but the screw dislocation cross slip affects it. Cross slip behavior is related to several lengths. For example, the screw part of the dislocation line must be long enough and the probability of cross slip occurring in the model is usually screw dislocation length dependent. Moreover, cross kink and double cross slip produce glissile junctions whose length is changeable, thus introducing new characteristic lengths into the screw dislocation-helium bubble interaction. We coarsen these physical processes into an effective characteristic length associated with cross slip depinning behavior. Accordingly, for screw dislocation, the characteristic length affecting hardening stress is not only related to helium bubble diameter and spacing, but also related to the dislocation characteristic length. Note that although the discussion above on the characteristic length is based on the interaction between a 5 nm helium bubble whose He/$V = 2$ and an edge or screw dislocation, it is applicable to a wide range of helium bubble size, spacing and temperature studied in this paper and for He/V inside the stable range, which will be explained in detail in the following sections

3.2. *Effect of He/V ratio*

Helium bubble may lead to different interaction behaviors when the ratio of helium atom to vacancy is varied. To understand this problem, we first carefully investigate the characteristics of the helium bubble itself for different He/V ratios. The configuration of helium bubbles with diameter of 3 nm and 5 nm and He/V from 0 to 5 are shown in Fig. 5, where tungsten atoms on the outer surface of

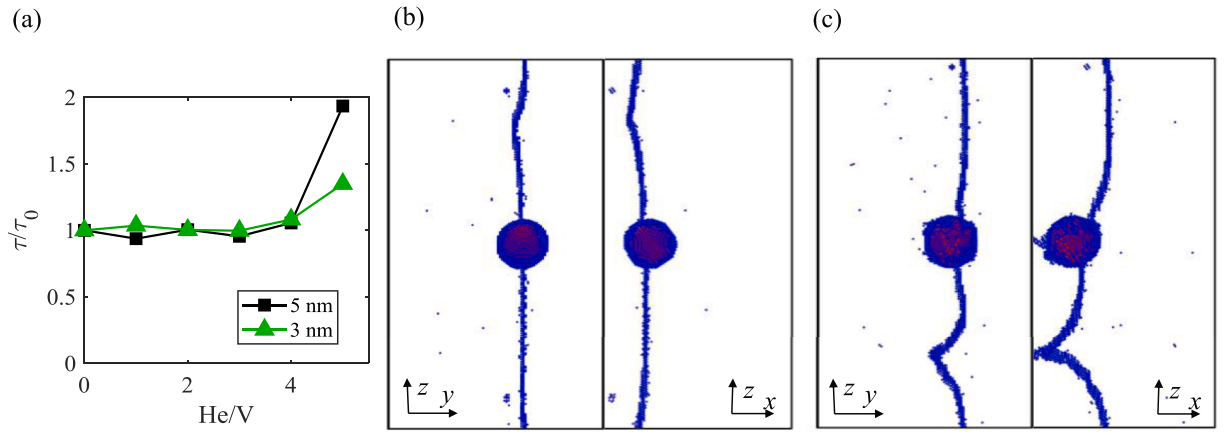

Fig. 7. (a) Normalized CRSS of screw dislocation interacting with helium bubbles of 3 nm and 5 nm with varied He/V ratios. τ_0 for 5 nm and 3 nm helium bubbles are 1067 MPa and 965 MPa, respectively. (b, c) Typical results show screw dislocation interacting with a helium bubble with He/V = 2 and 5, respectively.

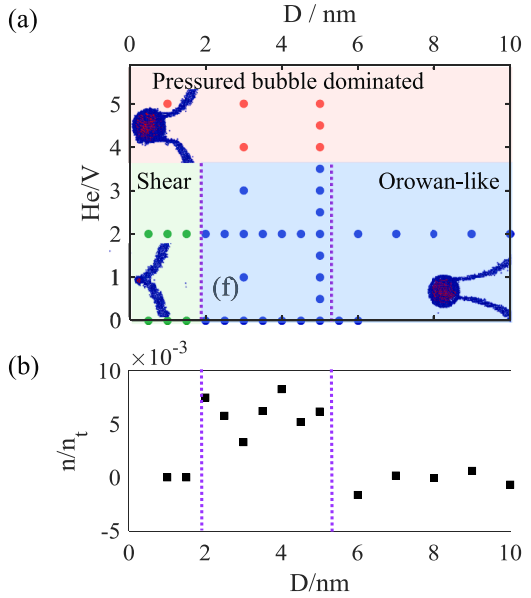

Fig. 8. (a) Phase diagram of the interaction mechanism between edge dislocation and helium bubble in the space of bubble size and He/V ratio. The colored dots denote the simulated cases. (b) The proportion of changed number of vacancies n to total vacancies n_t in 1~10 nm helium bubble. D is the diameter of helium bubble. The three regimes in (b) and the bottom half of (a) divided by the purple dotted line indicate that the interaction mechanism is shear, the interaction mechanism is Orowan-like and the changed vacancy complies with the square law, and the interaction mechanism is Orowan-like and the changed vacancy takes a small proportion, respectively.

the helium bubble are colored as blue and helium atoms are red. It is found that as the proportion of helium atoms to vacancies increases from 0 to 3, the shape of the helium bubble remains spherical and is nearly unchanged. When He/V = 5, the helium bubble is strongly over-pressurized due to the existence of a large number of helium atoms. Its shape changes from a highly symmetric sphere to some irregular shape that expands locally during the equilibration process, and the bubble volume expands. The result of He/V = 4 is between the above two cases. The helium bubble is basically spherical, but the surface shape is slightly different from that of helium bubble with low He/V. These results agree with the previous study of helium bubble's He/V ratio in tungsten (Faney, 2013; Li et al., 2014; Yi et al., 2017; Hammond et al., 2018; Zhan et al., 2019). For the inner helium pressure, it is about 28 GPa for a 5 nm helium when He/V = 5 and 5 GPa when He/V = 4, which is on the same order of magnitude as the data obtained from previous studies of pressured helium bubbles in tungsten (Ito et al., 2014; Cui et al., 2015; Huang et al., 2021), and lower than the critical pressure (0.2μ according to Wolfer, 1988) for helium bubbles to punch out a dislocation loop.

The influence of He/V ratio is reflected in two aspects, namely, the interaction mechanism and mechanical response. The CRSS of an edge dislocation overcoming helium bubbles with different He/V ratios is normalized by the case of He/V = 0 in Fig. 6(a). When He/

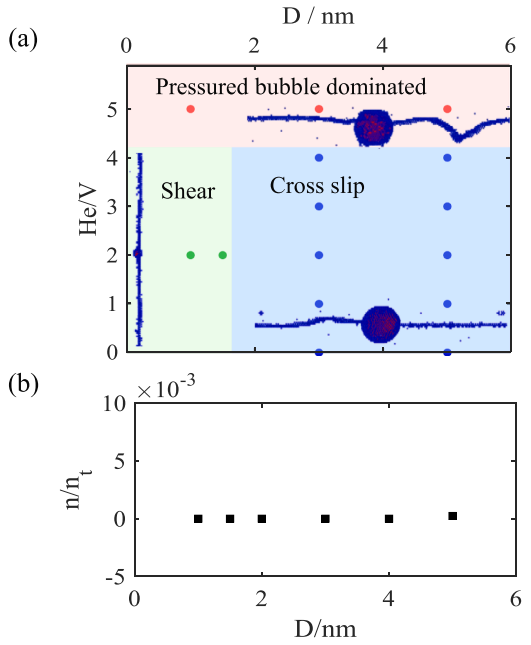

Fig. 9. (a) Phase diagram of the interaction mechanism between screw dislocation and helium bubble in the space of bubble size and He/V ratio. The colored dots denote the simulated cases. Three small insets in (a) are the configurations from the view perpendicular to the slip plane when the screw dislocation interacts with the helium bubble, reflecting the degree of cross slip of the screw dislocation. (b) The proportion of changed number of vacancies n to total vacancies n_t in 1~5 nm helium bubble.

V<4, the interaction process is the same as that exhibited in Fig. 3, implying that the interaction mechanism is not sensitive to He/V ratio. As for the mechanical response, He/V ratio has almost no effect on CRSS as shown in Fig. 6(a). The absence of He/V sensitivity in this range may be a result of their similar bubble surface configuration. When He/$V \geq 4$, CRSS decreases obviously with the increase of the He/V ratio. In this case, the helium bubble is over-pressured and lacks vacancy. It tends to absorb a lot of vacancies from the semi atomic plane of the edge dislocation, leading to a large degree of dislocation climb, as shown in Fig. 6(b). After climb, the heavily jogged dislocations no longer interact with the bubble in its equatorial plane, but near the periphery of the helium bubble. Thereby, the corresponding CRSS is much smaller. In the case of high He/V, the phenomenon that helium bubble absorbs vacancies from edge dislocation inducing a large degree of dislocation climb and a decrease in CRSS is also observed in BCC Fe (Hafez Haghighat and Schäublin, 2010; Osetsky and Stoller, 2015).

Similar to the case of edge dislocation, when He/$V \leq 4$, the interaction of the screw dislocation and helium bubble is not sensitive to the He/V ratio, and CRSS is nearly unchanged, as shown in Fig. 7(a). Since the screw dislocation has high lattice resistance and the helium bubble hardening stress is relatively low, the overall CRSS exhibits a weak stochastic feature due to the randomness of the cross-slip and dislocation glide path. When He/$V = 5$, the CRSS increased sharply, which is different from the corresponding case of edge dislocation. For He/$V \leq 4$, the degree of cross slip is small, and it is easy for screw dislocation to return to its original slip plane. However, in the situation of He/$V = 5$, cross kink easily appears, and the degree of cross slip is substantial, as shown in Fig. 7(c). High stress is required to drive the dislocation to return to its original slip plane and continue to glide.

Besides, at high He/V, spherical helium bubbles are largely distorted and their geometry symmetry is broken (Rigelesaiyin et al., 2018). The stress of atoms near the helium bubble is high and asymmetric. The complex local stress field in this scenario may also lead to their abnormal interaction mechanism and mechanical response.

3.3. Phase diagram of the interaction mechanism

In addition to He/V ratio discussed in Section 3.2, the size of helium bubble also influences the interaction mechanism between dislocation and helium bubble. To demonstrate their coupled effect, phase diagrams are given in this section for the case of edge and screw dislocation, respectively.

3.3.1. Edge dislocation-helium bubble interaction

The phase diagram is established in Fig. 8(a) to clarify the interaction mechanism between edge dislocation and helium bubble depending on the bubble size and He/V ratio.

As discussed previously, at a high He/V, dislocation-bubble interaction is pressured bubble dominated (see Fig. 6(b)), similar to the dislocation climb mechanism for helium bubble growth found by Xie et al. (2018). When He/V is not high (<4), the interaction mechanism and mechanical response do not change with He/V ratio variation. Bubble size dominates the interaction mechanism in

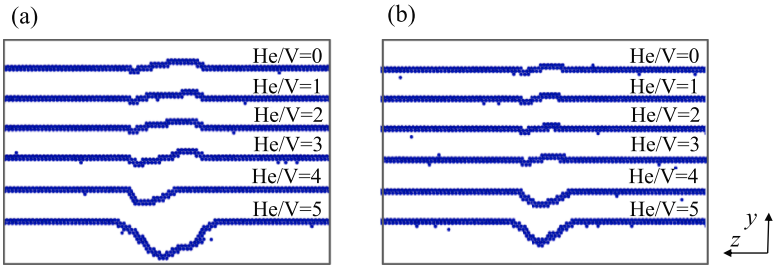

Fig. 10. Snapshots of the shape of climbed dislocation after interacting with helium bubble with He/V ratios ranging from 0 to 5 and size of (a) 5 nm and (b) 3 nm.

this range. If the size of helium bubble is smaller than 2 nm, two ends of the dislocation leave the helium bubble when the angle between them is still large and the line curvature is small. The interaction between dislocation and bubble is weak and no climb occurs. The interaction mechanism is shear, as helium bubble is simply sheared (Xu et al., 2019). The top half of the helium bubble is sheared with a distance equal to the magnitude of the Burgers vector along the dislocation glide direction, but the bottom half is unchanged, leaving surface steps on the "entry" and "exit" sides of the bubble. If the helium bubble is larger, dislocation bows out and is strongly pined to have a screw-like dipole in the vicinity of the bubble. In such a case, dislocation climb assists dislocation glide and depinning as described in Section 3.1. This mechanism is called Orowan-like because it is similar to the dipole configuration that occurs for the Orowan mechanism which involves impenetrable obstacles (Osetsky et al., 2003; Osetsky and Stoller, 2015; Yu et al., 2022). Similar transition from shear to Orowan-like is also observed for the interaction between edge dislocation and cavity in metals like molybdenum (Dutta et al., 2012), tungsten (Liu et al., 2004) etc.

3.3.2. Screw dislocation-helium bubble interaction

For the interaction between screw dislocation and helium bubble, a phase diagram similar to that for edge dislocation is summarized in Fig. 9(a). When He/V is high, screw dislocation has obvious kinks, the degree of cross slip is very large, and the interaction process is dominated by helium bubbles with high internal pressure. When He/V is in the stable range, if the helium bubble is very small, the screw dislocation directly cuts through the helium bubble and the interaction mechanism is shear. There is nearly no dislocation pinning and its motion is almost the same as that without bubble. With the increase of helium bubble size, screw dislocation is pinned and then released by the cross slip mechanism.

In summary, to obtain the mechanism of dislocation-helium bubble interaction, it is necessary to see whether the He/V ratio is greater than the stable range firstly. For high He/V, the interaction mechanism is dominated by over-pressured helium bubbles. Otherwise, the size of the helium bubble determines whether it is the shear or the Orowan-like mechanism for edge dislocation- helium bubble interaction, and the shear or cross slip mechanism for screw dislocation-helium bubble interaction.

As discussed above, He/V ratio of helium bubble in the stable range does not affect the interaction mechanism and mechanical response for both edge and screw dislocation interacting with the bubble, but high He/V does. However, at high helium-to-vacancy ratios (as the "pressured bubble dominated" area in phase diagrams), the helium bubble is mechanically unstable and its volume tries to expand, resulting in the actual He/V being smaller than the value set initially. Considering that the equilibrium ratio of He/V is smaller than 4, this situation is ignored during the following establishment of the kinetics and hardening models of helium bubbles.

4. Helium bubble kinetics model

The damage and destruction of irradiation defects caused by the interaction with dislocations are crucial inducements for the formation of defect-free channels and further irradiation embrittlement. Therefore, the kinetics of helium bubble due to their interaction with moving dislocation is a key problem to be investigated.

4.1. Bubble kinetics due to the interaction with edge dislocation

4.1.1. Mechanism dependent evolution behavior

The climb behavior of dislocations reflects the interaction mechanism between edge dislocations and helium bubbles. During climb, edge dislocations exchange vacancies with helium bubbles. Correspondingly, the number of vacancies in the helium bubble is changed, and the helium bubble shrinks or grows. It is not trivial to directly show the vacancy change of bubble after interaction, because a 3 nm helium bubble in tungsten contains nearly a thousand vacancies, and the variation number of the vacancies is so small relative to the total number of vacancies that it is difficult to be identified accurately. Therefore, the vacancy number change of bubble is measured by the shape of climbed dislocation line after interaction. We have verified that the error of changed vacancies number between that from climbed dislocation line and bubble configuration is tiny. Similar treatment is also used to investigate the change of vacancies in cavity, by studying the shape of climbed dislocation line after interaction (Osetsky and Bacon, 2003b; Hafez Haghighat and Schaeublin, 2008; Terentyev et al., 2008; Grammatikopoulos et al., 2011; Osetsky and Stoller, 2015; Osetsky, 2021).

Firstly the effect of He/V ratio on helium bubble evolution is evaluated, and climbed dislocation configurations after interacting

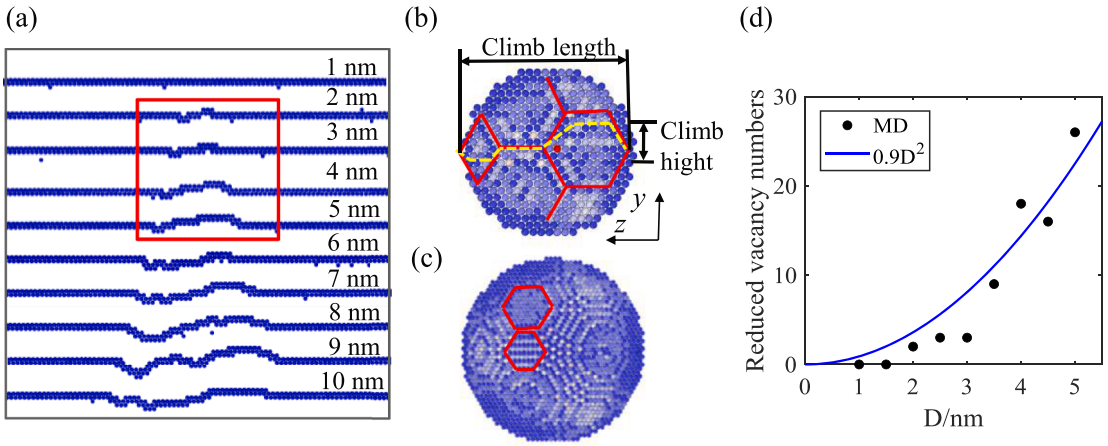

Fig. 11. (a) Snapshots of the climbed configuration of the dislocation after interaction with He/V = 2 helium bubble of size 1~10 nm. (b) The surface of a 5 nm helium bubble. Typical facets on it are highlighted by red lines and the dislocation path by dotted yellow lines. (c) The surface of a 10 nm helium bubble, and typical facets on it are highlighted by red lines. (d) Reduced vacancies of bubbles of size 1~5 nm and the fitted results by the square relationship.

with bubbles of different He/V ratios are presented in Fig. 10. It shows for He/V<4, the number of helium atoms has almost no effect on the climbed dislocation configuration feature. By contrast, for He/$V \geq 4$, the high-pressured helium bubble absorbs a lot of vacancies and expands in volume. This phenomenon is similar to the dislocation climb mechanism of helium bubble growth (Xie et al., 2018). As helium bubbles with high He/V ratio are unstable and thus be ignored, it can be concluded that in the considered range of He/V ratio, the change of vacancy number inside helium bubble before and after the interaction is insensitive to He/V, which indicates that He/V in the stable range does not affect the kinetics of helium bubbles.

For the influence of helium bubble size, when the helium bubble size is small (such as 1 nm) and the interaction mechanism is shear, the dislocation does not climb. There is no vacancy exchange between the dislocation and the helium bubble, and the helium bubble volume remains unchanged. With the increase of helium bubble size, the dislocation is released by climb, and the helium bubble evolves. As shown in Fig. 11(a), when the size of the helium bubble ranges from 2 nm to 5 nm, the dislocation overall climbs up. Its upper semi atomic plane becomes smaller, indicating the edge dislocation absorbing vacancies. Correspondingly, the helium bubble loses vacancies and shrinks. When the size of the helium bubble is greater than 5 nm, the climb direction of the dislocation becomes uncertain, indicating that the helium bubble may shrink or grow after interaction.

4.1.2. Quantitative model

Based on the physical process of edge dislocation-helium bubble interaction, a quantitative model for bubble evolution is established here.

Helium bubble is not perfectly spherical due to its lattice structure, and it is made up of facets with hexagons and quadrilaterals on the surface, which is similar to void whose surface after relaxation is composed of polygonal {110} planes with edges along <112> directions and {100} planes to minimize the surface energy (Huang et al., 2021; Yu et al., 2022). When the dislocation interacts with these helium bubbles of different sizes, dislocation tends to climb along the same path, as marked by the dotted yellow line in Fig. 11 (b). It is found that the climbed configurations of dislocations after interacting with helium bubbles of different sizes are self-similar for helium bubble with size among 2~5 nm. Typical results are marked by the red box in Fig. 11(a). As the size of helium bubble increases, both climb length and height increase, as shown in Fig. 11(b). Hence the number of vacancies change in helium bubble is proportional to the square of the bubble size. The vacancy change of bubble from MD is counted, and it is found that the square law is indeed satisfied, as shown in Fig. 11(d). On the other hand, because of the shear mechanism of the small helium bubble and edge dislocation interaction, the small bubble does not change in volume, and the vacancy change should be zero. Since the value of quadratic function is very close to zero when the bubble diameter is close to zero, it is acceptable to use the same relation. Therefore, for convenience, it can be considered that the quadratic function can describe the kinetics of helium bubbles with sizes from 0 to 5 nm.

Larger bubble size allows for smaller and multilevel facets of {110} and {100} planes. For example, as shown in Fig. 11(c), for a helium bubble with size larger than 5 nm, there are small polygonal facets between the large facets on the surface of the helium bubble, which is similar to the fractal structure. Consequently, the climbed dislocation configuration is no longer self-similar to that of 2~5 nm, and the number of changed vacancies no longer satisfies the quadratic function. This implies that the change of bubble surface characteristics alters the climb path of the dislocation on bubble surface and thus changes the kinetics of helium bubble.

As the total number of vacancies in the helium bubble increases rapidly with increasing of the size, the proportion of changed vacancies in the helium bubble larger than 5 nm is very small (<0.2%), as shown in Fig. 8(b), which can be almost ignored. In addition, most of the helium bubbles produced in bulk tungsten from experiments are less than 5 nm in size (Nishijima et al., 2004; Harrison et al., 2017; Kong et al., 2017; Ipatova et al., 2021), and the probability of more giant helium bubbles is very low. Consequently, a helium bubble kinetics model for the edge dislocation and helium bubble interaction is established as follows,

$$\frac{\Delta D}{D}=\begin{cases}\left(1-\frac{\beta d}{D}\right)^{\frac{1}{3}}-1, & \text{if } D\le D_{crit}\\ 0, & \text{if } D>D_{crit}\end{cases} \tag{1}$$

where $D=\sqrt[3]{6n_t\Omega/\pi}$ is the current bubble size. n_t is the total vacancy number in bubble and Ω is the vacancy volume. ΔD is the change of bubble diameter after interaction with dislocation. d is the vacancy diameter and $d=\sqrt[3]{6\Omega/\pi}$. D_{crit} is the critical size as 5 nm and β is fitted as 0.086 according to the curve in Fig. 11(d). For the influence of temperature on helium bubble kinetics, temperatures ranging from 10 to 900 K are simulated. It is found that helium bubble kinetics caused by the edge dislocation-helium bubble interaction is weakly temperature-dependent, and a detailed evaluation of the temperature effects will be studied further.

This model can be degenerated to the evolution of voids in tungsten. Our MD results demonstrate that the fundamental process of dislocation-bubble interaction is consistent with that of dislocation-void interaction (Osetsky, 2021; Yu et al., 2022). Based on the analysis above, we try to answer the controversial question of void kinetics during the dislocation-void interaction mentioned in the introduction. After interaction with 5 nm and 6 nm bubbles, edge dislocations are overall upward and downward climbed as shown in Fig. 11(a), indicating a slight shrinkage and expansion of helium bubble, respectively. These results are consistent with previous simulations at the corresponding size (Osetsky, 2021; Yu et al., 2022) that 5 nm voids lose vacancy but 6 nm voids gain vacancy after interacting with edge dislocations. We conjecture that the different directions of dislocation climb after interaction with different sizes of helium bubbles are due to the change in bubble surface facets described above.

4.2. Bubble kinetics due to interaction with screw dislocation

As screw dislocation does not climb, there is no vacancy exchange between screw dislocation and the helium bubble, and the volume of helium bubble remains unchanged. In addition, even though the cross slip behavior of screw dislocations may leave defect clusters (Cui et al., 2016), the probability of leaving interstitial debris or vacancy debris is the same, so the cross slip does not affect the volume of the helium bubble from a macroscopic perspective. Therefore, the interaction between screw dislocation and helium bubble does not lead to the evolution of helium bubble. Fig. 9(b) shows the ratio of vacancy change of the helium bubble to the total vacancy it contains before and after the interaction with the screw dislocation, which also verifies the conclusion that the screw dislocation does not affect the kinetics of helium bubble.

5. Hardening and yield strength model incorporating helium bubble

Hardening is one of the most crucial irradiation effects of helium bubble as it blocks dislocation movement. In this section, considering the dislocation-bubble interaction mechanism, a unified hardening model for edge, screw and mixed dislocation is proposed. The yield strength model of irradiated tungsten is further developed to consider the thermal activated mechanism of dislocation activities. As discussed in Section 3.2, He/V ratio in the stable range does not affect mechanical response of dislocation-bubble interaction, thus the hardening and yield strength model is independent of He/V.

5.1. Unified hardening model

To the best of our knowledge, there is no hardening model yet that is carefully verified to be able to simultaneously predict the hardening of edge, screw, and mixed dislocations hindered by helium bubble. Here, a hardening model for arbitrary dislocation types is developed.

Based on the analysis in Section 3.1, the hardening stress is correlated with several characteristic lengths including the bubble diameter D and spacing L, as well as the dislocation characteristic length L_D corresponding to the cross slip depinning mechanism for screw dislocation. The two characteristic lengths of helium bubble diameter and spacing can be integrated into one effective characteristic length of bubble as L_B, which appropriately represents the outer cut-off or screening distance for dislocation stress field during the dislocation interacting with the bubble (Bacon et al., 1973). When L is small compared to D, the dislocation segments separated by helium bubbles are far away from each other during interaction, thus the dislocation between two adjacent bubbles should behave as an isolated line, and $L_B \approx L$. When D is small compared to L, on the other hand, the dislocation segments near a bubble should interact strongly with the segments on the other side of the obstacle, and it seems reasonable to suppose $L_B \approx D$. The most straightforward average of D and L with the proper limiting behavior is a harmonic mean, thus $L_B = 1/(D^{-1}+L^{-1})$. Accordingly, the comprehensive characteristic length for hardening L_H is defined as the norm of bubble characteristic length L_B and dislocation characteristic length L_D, namely $\left(\frac{1}{L_H}\right)^n=\left(\frac{1}{L_B}\right)^n+\left(\frac{1}{L_D}\right)^n=(D^{-1}+L^{-1})^n+(L_D^{-1})^n$ with $n=1/2$. In this way, based on the form of Orowan stress, helium bubble hardening is expressed as

$$\tau_H=\frac{\mu b}{2\pi L}\left[\ln\left(\frac{L_H}{r_0}\right)+\Delta\right] \tag{2}$$

where τ_H represents the hardening stress (increase of the CRSS with respect to the case without irradiation defect) necessary to unlock a dislocation from a bubble. L is the bubble spacing taken as the bubble center's distance minus the bubble diameter, representing the

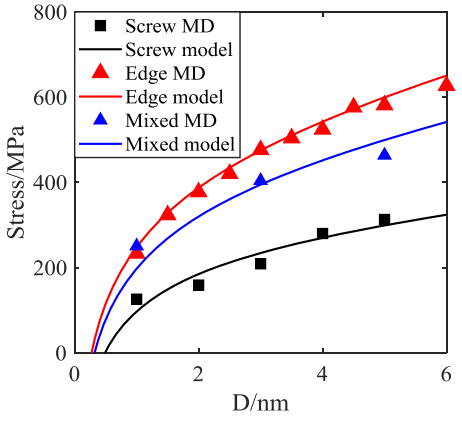

Fig. 12. Hardening stress τ_H of screw, edge and mixed dislocation from bubble of He/$V = 2$ as a function of bubble diameter D from MD simulation (points) and predicted by the proposed model (lines).

distance between two pinning points of a dislocation line in MD simulation. μ is the shear modulus and b is the Burgers vector magnitude. r_0 is the cut-off distance or dislocation core radius, which is determined by b here (Osetsky and Bacon, 2003b; Xu et al., 2019; Yu et al., 2022). Δ is the dimensionless coefficient related to bubble surface energy (Scattergood and Bacon, 1982; Osetsky, 2021), and it reflects the defect strength.

For edge dislocation, it does not cross slip thus L_D is set as ∞. In this way, $L_H = L_E = 1/(D^{-1} + L^{-1})$. Here, L_E is the comprehensive characteristic length L_H in the case of edge dislocation-helium bubble interaction. Eq. (2) degenerates to the Bacon–Kocks–Scattergood (BKS) hardening model (Bacon et al., 1973; Scattergood and Bacon, 1982; Osetsky and Bacon, 2010), which is preferred for describing spherical defects like voids and precipitations (Osetsky and Bacon, 2003b; Bacon and Osetsky 2005),

$$\tau_{H\_Edge} = \frac{\mu b}{2\pi L}\left[\ln\left(\frac{L_E}{r_0}\right) + \Delta\right] = \frac{\mu b}{2\pi L}\left[\ln\left(\frac{1}{r_0\left(D^{-1} + L^{-1}\right)}\right) + \Delta\right] \tag{3}$$

Using the current MD results of edge dislocation interacting with helium bubbles of He/$V = 2$ and different diameters D, the parameter Δ is fitted as 0.0, which is close to 0.006 from Yu et al. (2022), and higher than −0.7 obtained by Osetsky (2021).

For screw dislocation, $L_H = L_S = \left(\frac{1}{(D^{-1}+L^{-1})^n + (L_D^{-1})^n}\right)^{\frac{1}{n}}$. Here, L_S is the comprehensive characteristic length L_H in the case of screw dislocation-helium bubble interaction. Eq. (2) becomes

$$\tau_{H\_Screw} = \frac{\mu b}{2\pi L}\left[\ln\left(\frac{L_S}{r_0}\right) + \Delta\right] = \frac{\mu b}{2\pi L}\left[\ln\left(\frac{1}{r_0\left(\left(D^{-1} + L^{-1}\right)^n + \left(L_D^{-1}\right)^n\right)^{1/n}}\right) + \Delta\right] \tag{4}$$

where L_D is fitted as 4.32 nm for tungsten using our MD results.

For a dislocation with an angle θ between the Burgers vector and the line direction, it can be decomposed into the combination of edge and screw dislocations, and the corresponding hardening stress can be expressed as

$$\tau_H = \cos^2\theta\tau_{H\_screw} + \sin^2\theta\tau_{H\_edge} \tag{5}$$

which can be further derived and simplified as

$$\tau_H = \frac{\mu b}{2\pi L}\left(\ln\left(\frac{L_E}{r_0}\right) + \cos^2\theta\ln\left(\frac{L_S}{L_E}\right) + \Delta\right) \tag{6}$$

where L_E and L_S are $L_H = \frac{1}{((D^{-1}+L^{-1})^n + (L_D^{-1})^n)^{1/n}}$with L_D set as ∞ and 4.32 nm, respectively. The dimensionless parameter Δ is 0.0. This method of decomposing the mixed dislocation into the combination of edge type and screw type components by using the square relation of trigonometric function through the angle between the dislocation line and the Burgers vector is also widely used to obtain other characters of mixed dislocations, such as dislocation velocity (Po et al., 2016). Eq. (6) can be degenerated to the extreme cases of screw and edge dislocations with θ equal to 0° and 90°, and is therefore a unified model applicable to various types of dislocations.

To verify the ability of this model to predict the hardening stress of dislocations interacting with helium bubbles, MD results of hardening stress of edge, screw and mixed dislocation interacting with helium bubbles at different sizes are compared with the prediction results from Eq. (6), as shown in Fig. 12. The simulation set up for the mixed dislocation is similar to the description in Section 2, with its slip plane being $[\bar{1}10]$, Burgers vector being [111] and line direction being [001]. It is clear that MD and the predicted results are in good agreement for different types of dislocations, which confirms the ability of the proposed model to predict helium bubble hardening. The applicability of the developed hardening model to different helium bubble spacings is verified in Appendix B,

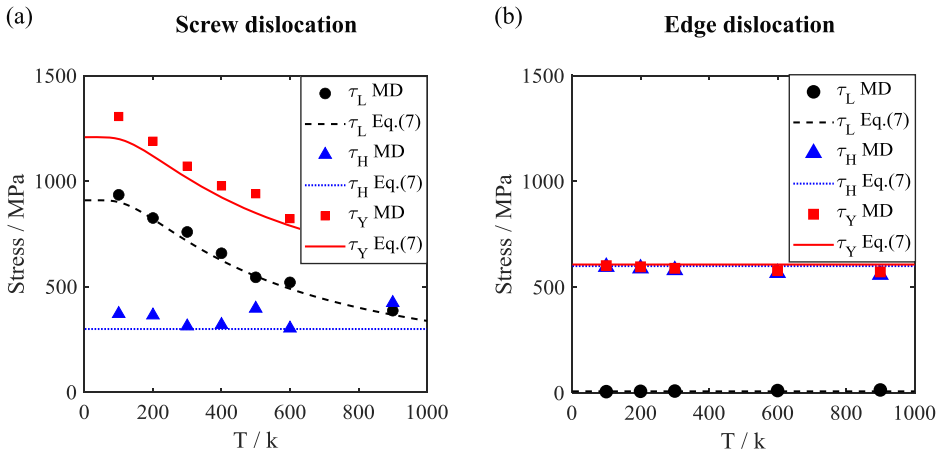

Fig. 13. Lattice resistanceτ_L, hardening stressτ_H, and yield stress τ_Y of (a) screw and (b) edge dislocation depinning from 5 nm bubble of He/$V = 2$ as a function of temperature T from MD simulation and the proposed thermal-activated models, respectively.

indicating that it performs well. It is worth pointing out that the hardening model established here can also be directly applied to voids hardening in tungsten or other materials with other irradiation defects such as precipitates by re-adjusting the parameters.

5.2. *Temperature dependent yield strength model*

In order to make the helium bubble hardening model be able to directly predict the mechanical response of irradiated tungsten, a temperature dependent yield strength model is further developed.

The first question is whether the bubble hardening is sensitive to temperature. We studied the edge and screw dislocations interacting with a 5 nm helium bubble at different temperatures ranging from 100 K to 900 K, and the hardening stress is shown as blue marks in Fig. 13(a) and (b), which shows that the hardening stress for both edge and screw dislocation has almost no temperature dependence. Therefore, it can be regarded that helium bubble hardening is not sensitive to temperature in the considered temperature range, and the proposed hardening model in Section 5.1 can be applied to temperatures ranging from 100 K to 900 K.

The second question is how to incorporate the inherent strong temperature dependent plasticity of tungsten. The hardening stress caused by the interaction with the helium bubble plus the inherent lattice resistance of dislocation is the CRSS of dislocation-bubble interaction, which also can be considered as the yield stress of irradiated material with the existence of irradiation-induced helium bubble. As previously discussed, hardening stress is not sensitive to temperature, but the lattice resistance of screw dislocation decreases with increasing temperature due to its thermally activated glide behavior. Generally, the lower the temperature is, the more difficult it is to move the screw dislocation and the slower the glide speed is. Relatively speaking, the influence of temperature on edge dislocation motion is much weaker than that of screw dislocation.

Based on previous MD and theoretical studies (Li et al., 2021; Lu et al., 2021), a thermally activated model is built to predict the release stress of interaction between bubble with edge and screw dislocation, as

$$\tau_{Y\_E/S} = \frac{\mu b}{2\pi L}\left[\ln\left(\frac{L_{E/S}}{r_0}\right) + \Delta\right] + \left[1 - \exp\left(-\frac{\Delta G}{2k_B T}\right)\right]\mu C_{E/S} \tag{7}$$

where the subsript *E/S* corresponds to edge or screw dislocations. The first term on the right side of Eq. (7) is the hardening stress τ_H and the second term denotes temperature dependent lattice resistance. L_E and L_S are expressed in Eq. (3) and Eq. (4), respectively. ΔG represents the free enthalpy of kink-pair nucleation (Po et al., 2016), which is fitted as 0.04 eV from MD data. C_E and C_S are dimensionless parameters set as 0.0 and 0.005 for edge and screw dislocation, respectively. k_B is the Boltzmann constant. T is temperature in Kelvin and μ is the shear modulus.

In order to verify the effectiveness of the proposed model, the prediction results are directly compared with MD results. As shown in Fig. 13, the temperature-dependent model performs well for both edge and screw dislocation cases. In addition to irradiation hardening, this model can also be degenerated to predict the yield strength of unirradiated tungsten.

6. Application of the proposed models

The atomistic mechanism informed bubble kinetics and hardening models proposed in Sections 4 and 5 can be directly used in micro and mesoscopic scale simulations such as discrete dislocation dynamics (DDD) and crystal plasticity (CP). In addition, the hardening model can directly predict the macroscopic experimental results at different temperatures.

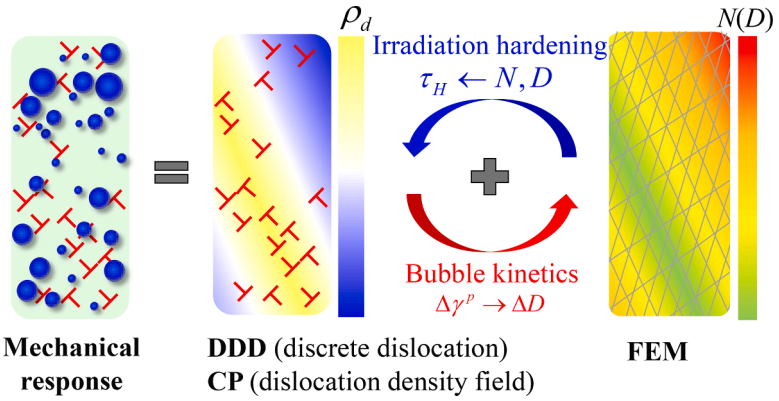

Fig. 14. Diagram of irradiation material mechanical response and the application strategy of established hardening and bubble kinetics model into DDD and CP irradiation simulation. ρ_d is the dislocation density. N and D are helium bubble density and average diameter, respectively. $\tau_H$is hardening stress from bubble expressed in Eq. (6) . $\Delta\gamma^p$ and ΔD are increment of plastic strain and bubble diameter, respectively.

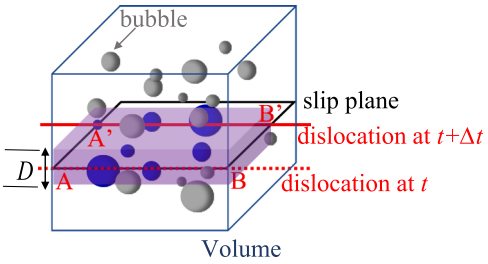

Fig. 15. Helium bubble damage graphic. The red line is a dislocation whose slip plane is plane on points A, B, B' and A'. The color of bubbles represents if they can interact (blue) or not (gray) with the dislocation. D is the average diameter of bubbles in this volume.

6.1. Application to multiscale simulation

The kinetics and hardening model developed in Sections 4 and 5 can be directly applied to DDD and CP models if the irradiation defects are described using continuum barrier field characterized by their density and mean size (Cui et al., 2018b). This kind of method can overcome the difficulty of the excessive number of equations to be solved (several hundred thousands) when the irradiation defects are described in a discrete manner, and it significantly improves computational efficiency. It performs well in investigating the irradiation hardening and plastic deformation localization behaviors of irradiated materials (Cui et al., 2018a; Li et al., 2021; Ji et al., 2022).

The essential idea of the method is schematically shown in Fig. 14. The interactions and evolution between dislocations are handled in DDD or CP. DDD directly considers the discrete dislocation segments and CP deals with the continuous dislocation density fields. The evolution of helium bubbles is calculated by the finite element method (FEM) based on their kinetics model described using density N and average size D. FEM transmits the spatially-dependent density and size of helium bubble to DDD or CP, and calculates the hardening stress caused by the helium bubble, as a resistance term of dislocation glide. DDD or CP transfers the plastic strain increment generated by dislocation slip to FEM, so as to calculate the damage and evolution of helium bubble during plastic deformation.

In the following, we will further discuss how to use the developed models in DDD and CP based methods, respectively.

6.1.1. Application to dislocation dynamics method

DDD is a tool to calculate and track the motion of dislocations, consider the short-range and long-range interactions between dislocations, and evaluate the plastic deformation induced by the collective motion of dislocations (Cui et al., 2017; Ghoniem and Cui, 2020; Cui et al., 2021; Guo et al., 2021; Dong et al., 2022; Lu et al., 2022). It can capture the interaction mechanism between dislocations and irradiation defects, get the collective interaction of dislocations, and obtain the macroscopic mechanical response of irradiated materials., thus is an effective tool to study irradiation effects.

In DDD, dislocation lines are discretized into a succession of parametrized segments. Dislocation segments may be screw, edge or mixed type, with a specific angle between the line direction and the Burgers vector. Therefore, the developed bubble hardening model applicable to different types of dislocation can be directly used to describe the barrier effect of helium bubble on dislocation motion, which can be used as follows,

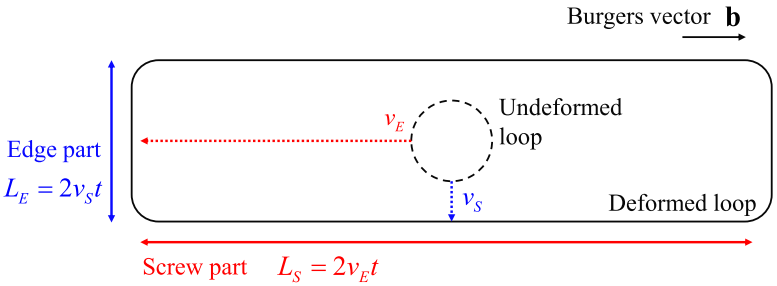

Fig. 16. Schematic showing the evolution process of screw and edge parts during the expansion of a dislocation loop (Li et al., 2021).

$$\boldsymbol{\sigma}_{irra} = \begin{cases} -\tau_H(\mathbf{b_s}\otimes\mathbf{n}+\mathbf{n}\otimes\mathbf{b_s})\mathrm{sign}(\tau_{glide}), & \text{if } |\tau_{glide}| > \tau_H \\ -\tau_{glide}(\mathbf{b_s}\otimes\mathbf{n}+\mathbf{n}\otimes\mathbf{b_s}), & \text{if } |\tau_{glide}| \le \tau_H \end{cases} \tag{8}$$

where $\mathbf{b_s}$ and $\mathbf{n}$ are the unit vectors of the Burgers vector and slip plane normal vector of the dislocation segment, respectively. $\otimes$ represents tensor product. τ_{glide} is proportional to peach-koehler (PK) force in the absence of irradiation defects. Here τ_H is hardening from irradiation-induced helium bubble expressed in Eq. (6).

The helium bubble damage caused by the edge part of the dislocation passing the helium bubble once is shown in Eq. (1). Plastic strain increment from dislocation glide is transferred from DDD to the continuous irradiation defect field. To consider the damage of bubble field as a function of plastic strain, it is assumed that only bubbles with a distance less than $D/2$ from the slip plane of the moving dislocation can be cut through (Ji et al., 2022), as shown in Fig. 15. For a time increment of Δt, if the slip area increment of the dislocation is ΔA, then the proportion of bypassed bubbles during the interaction is $D\Delta A/V$, which is equal to $D\Delta\gamma^p/b$ according to Orowan relation. Thus, for the specific control volume V, the evolution of bubble diameter can be expressed as

$$\begin{cases} \dfrac{\Delta D}{D} = \left(1-\dfrac{\beta\Delta\gamma^p d}{b}\right)^{\frac{1}{3}} - 1, & \text{if } D \le D_{crit} \\ \dfrac{\Delta D}{D} = 0, & \text{if } D > D_{crit} \end{cases} \tag{9}$$

In order to avoid the situation that the helium bubble size is negative after the reaction, if the helium bubble size is less than $D_{eff} = \beta d$, the corresponding void diameter after one time of interaction is $D' = (D^3 - \beta D^2 d)^{1/3} = 0$ in actual calculation. It is considered that the dislocation will absorb it and the corresponding helium bubble density will decrease. In this case, $\Delta D = 0$ and $\Delta N = -ND\Delta\gamma^p/b$. It means that bubbles smaller than D_{eff} are entirely destroyed after one interaction process and thus causing bubble density to deduce. The corresponding physical process is similar to that of dislocation absorbing a single vacancy (Chen et al., 2011; Li et al., 2019). While for the medium size ones, interaction only decreases their size, as expressed in Eq. (9). Therefore, the comprehensive bubble kinetics model is

$$\begin{cases} \dfrac{\Delta N}{N} = -\dfrac{D\Delta\gamma^p}{b}, & \text{if } D < D_{eff} \\ \dfrac{\Delta D}{D} = \left(1-\dfrac{\beta\Delta\gamma^p d}{b}\right)^{\frac{1}{3}} - 1, & \text{if } D_{eff} \le D \le D_{crit} \\ \dfrac{\Delta D}{D} = 0, & \text{if } D > D_{crit} \end{cases} \tag{10}$$

6.1.2. Application to crystal plasticity model

For CP, dislocations are characterized by dislocation density fields in different slip systems (Das et al., 2020; Wang et al., 2020; Wen et al., 2020; Liu et al., 2022). The coupling operation and parameter transformation are consistent with the consideration of DDD coupling helium bubble field, as shown in Fig. 14. The main difference is that the mixed dislocation needs to be directly treated in DDD, while in CP one generally does not need to calculate the exact angle between the Burgers vector and line direction of dislocation lines, and only cares about the total dislocation density, or the edge or screw dislocation density.

Understanding the temperature-dependent plastic behavior of tungsten is essential for studying its mechanical response with helium bubbles and then compare with experiments. At low temperatures, screw dislocation is difficult to slip in BCC metals, but the edge dislocation is easy to glide with a much faster speed. Therefore, many screw dislocations are left inside the crystals, and the plastic deformation of tungsten is dominated by screw dislocations at low temperatures. With the increase of temperature, the remark difference in mobility between screw dislocation and edge dislocation gradually disappears, then there is no need to distinguish edge and screw dislocation.

In order to develop a unified model, one needs to describe the temperature dependent screw and edge dislocation density. Based on

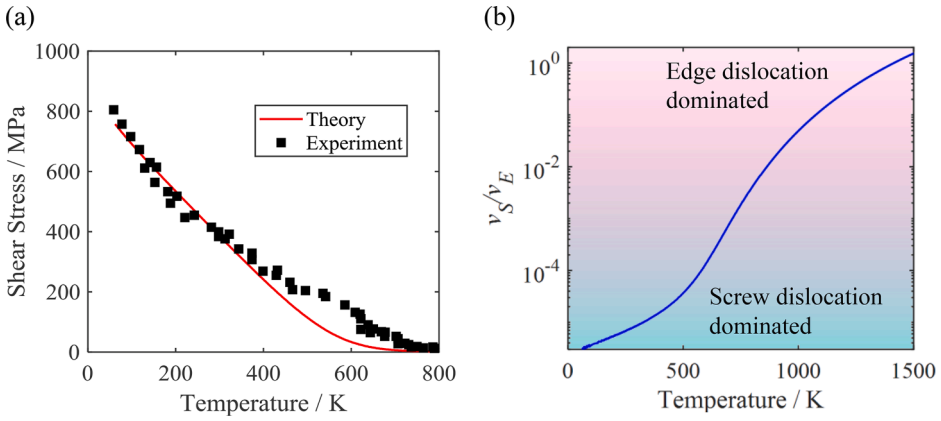

Fig. 17. (a) Comparison of theory results and experimental data (Brunner, 2010) on the flow shear stress as a function of temperature of tungsten at an applied strain rate of $8.5 \times 10^{-4}/s$. The dislocation density is $5.5 \times 10^{9}/m^2$, and loading orientation is $[\bar{1}24]$. (b) Ratio of screw dislocation velocity v_S to edge dislocation velocity $v_E$with the change of temperature.

the analysis of dislocation loop evolution process shown in Fig. 16 (Li et al., 2021), the multiplication ratio ϑ between the edge and screw dislocation can be approximately expressed as $\vartheta = v_S/v_E \approx L_E/L_S$, where v_S and v_E are velocity of screw and edge dislocation, respectively. The length of screw dislocations and edge dislocations is $2L_E$ and $2L_S$. In this way, the density of edge dislocation ρ_E with respect to that of screw dislocation ρ_S is approximately v_S/v_E. Dislocation velocity is theoretically calculated by its thermal-activated mobility law, which is a function of stress state and temperature. Using the phenomenological dislocation mobility law for tungsten described in detail in (Po et al., 2016) and the Orowan relationship, the required shear stress for a sample of dislocation density $5.5 \times 10^{9}/m^2$ to achieve a plastic strain rate of $8.5 \times 10^{-4}/s$ at different temperatures is gained, as shown in Fig. 17(a). The predicted yield stress matches well with the experimental data using the same parameters (Brunner, 2010). Based on these results and using the dislocation mobility law again, the ratio of screw dislocation velocity to edge dislocation velocity under temperature-dependent yield stress is obtained, as shown in Fig. 17(b). v_S/v_E is small at low temperatures, and vice versa at high temperatures. In CP, the evolution equation of screw and edge dislocation density is expressed as $\dot{\rho}_S = (k_1\sqrt{\rho_S}/b - k_2\rho_S)\dot{\gamma}^p$ and $\dot{\rho}_E = (\vartheta k_1\sqrt{\rho_E}/b - k_2\rho_E)\dot{\gamma}^p$, respectively, where k_1 and k_2 are parameters associated with the generation and annihilation process of dislocations, respectively. As a multiplication ratio, ϑ controls the evolution of dislocation density and ultimately the equilibrium density of edge and screw dislocations.

If edge and screw dislocations are not distinguished in CP model, the ratio of their velocity can be simply evaluated by the method getting Fig. 17(b), then the ratio of dislocation density can be estimated by $\vartheta = v_S/v_E \approx L_E/L_S$. If the density of edge and screw dislocations is distinguished and calculated, following the coupling strategy of CP and FEM shown in Fig. 14, the hardening and bubble kinetics models of edge and screw dislocations are applied to them, respectively. Specifically, the resistance stress of helium bubbles on dislocation motion can be obtained by Eqs. (3) and (4), respectively. The effect of the edge dislocation motion on the helium bubble is gained using Eq. (10), while screw dislocation does not lead to bubble evolution.

6.2. *Application to predict experimental results*

Furthermore, the hardening model proposed in this work can be directly employed to predict the hardening behavior of irradiated materials. The complexity of predicting experimental results lies in the possibility of coexistence of multiple types of irradiation defects. For tungsten, typical irradiation defects include interstitial loops and helium bubbles (or voids) (Koyanagi et al., 2017; Huang et al., 2021; Shi et al., 2022). Therefore, it is necessary to establish a model which takes into account the effect of different defects collectively hindering dislocation motion.

The combined effect of interstitial loop and helium bubble on hardening can be expressed as $\Delta\tau = \sqrt{\tau_{IL}^2 + \tau_H^2}$, namely the 1/2 power of the sum of squares of the hardening stress from interstitial loops and helium bubbles (Sobie et al., 2015; Weaver et al., 2017).

Since most of the existing mechanical response of irradiated tungsten is obtained based on indentation experiments, the formula to predict the defect induced hardness can be expressed as

$$\Delta H = k\Delta\sigma = \frac{k}{m}\sqrt{\tau_{IL}^2 + \tau_H^2} \tag{11}$$

where the increase of hardness is proportional to the increase of yield stress with a scale factor $k = 3.20$ for tungsten (Hu et al., 2016), close to the parameter for Vickers hardness in previous works (Yan 2006; Pavlina and Van Tyne 2008; Zhang et al., 2011). This parameter is not only applicable to Vickers hardness measurement, but can also be used to the experiment of spherical nanoindentation (Weaver et al., 2017), covering all experimental methods in the following comparison. m is the Schmid factor. τ_{IL} is hardening stress induced by interstitial loops expressed as $\tau_{IL} = \alpha_{DBH}\mu b\sqrt{N_{IL}D_{IL}}$ with the parameter α_{DBH} set as 0.3 (Cui et al., 2018b; Cui et al., 2021). N_{IL} and D_{IL} are density and diameter of interstitial loops, respectively. τ_H is hardening stress from helium bubble proposed in Section 5.

Table 1
Experimental irradiation defect data and hardness increase from indentation experiments and prediction from Eq. (11) of tungsten and relevant alloys.

Material	Irradiation	T /K	*Dose* /dpa	Irradiation loop		Bubble(void)		Hardness increase ΔH /GPa		Relative error	Ref.
				N_{IL} /m^3	D_{IL} /nm	N /m^3	D /nm	Experiments	Predicted		
W	He +*W*	298	1	3.00×10^{22}	3.0	9.10×10^{23}	1.1	1.9,2.7, 5.5,7.3	4.4	–	(Weaver et al., 2017)
W	neutron	298	0.15	7.00×10^{20}	14.8	3.40×10^{22}	2.8	1.5	1.4	7%	(Shi et al., 2022)
W	neutron	298	0.18	5.80×10^{20}	5.3	1.90×10^{22}	4.0	1.1	1.4	27%	(Shi et al., 2022)
W	neutron	298	0.42	1.10×10^{21}	5.6	1.22×10^{23}	2.45	2.2	2.3	5%	(Shi et al., 2022)
W	neutron	298	1.54	6.00×10^{21}	20.0	1.20×10^{23}	4.7	3.3	4.2	27%	(Shi et al., 2022)
W	neutron	673	0.17	2.00×10^{22}	2.8	1.95×10^{23}	1.8	2.1	2.3	10%	(Hu et al., 2016)
W	neutron	804	0.44	1.10×10^{22}	5.4	2.53×10^{23}	1.3	1.7	1.9	12%	(Hu et al., 2016)
W	neutron	804	0.44	1.30×10^{22}	7.5	1.90×10^{23}	1.1	1.7	1.7	0%	(Fukuda et al., 2012)
W	neutron	811	0.96	4.70×10^{22}	4.7	4.90×10^{23}	2.1	3.6	4.3	19%	(Hu et al., 2016)
W	neutron	856	0.47	2.00×10^{21}	5.4	1.38×10^{23}	2.4	3.0	2.4	20%	(Hu et al., 2016)
W	neutron	856	0.47	2.0×10^{21}	3.0	1.28×10^{23}	3.1	3.0	2.9	3%	(Fukuda et al., 2012)
W	neutron	873	0.15	4.60×10^{21}	7.9	6.40×10^{22}	1.3	2.1	2.4	14%	(Hu et al., 2016)
W	neutron	873	0.15	4.60×10^{22}	7.9	6.40×10^{22}	1.3	2.1	2.4	14%	(He et al., 2006)
W	neutron	973	0.15	7.00×10^{21}	7.4	3.40×10^{22}	1.4	1.7	1.1	35%	(He et al., 2006)
W	neutron	983	0.70	2.40×10^{22}	2.2	3.00×10^{21}	4.1	3.1	1.0	68%	(Fukuda et al., 2016)
W	neutron	1013	0.40	3.00×10^{21}	12.2	1.27×10^{23}	2.9	2.1	2.8	33%	(Hu et al., 2016)
W	neutron	1029	0.42	1.00×10^{21}	5.6	1.21×10^{23}	2.5	1.7	2.4	41%	(Hu et al., 2016)
W	neutron	1073	0.15	1.10×10^{21}	8.5	4.20×10^{22}	1.9	1.7	1.6	5.8%	(Hu et al., 2016)
W	neutron	1073	0.15	4.80×10^{22}	2.0	2.00×10^{21}	3.9	1.2	1.2	0%	(Fukuda et al., 2016)
W	neutron	1073	0.15	1.10×10^{22}	8.5	4.20×10^{22}	1.9	1.5	1.6	7%	(He et al., 2006)
W-3%*Re*	neutron	804	0.44	4.60×10^{22}	3.7	3.00×10^{20}	1.4	0.7	1.5	114%	(Fukuda et al., 2012)
W-3%*Re*	neutron	856	0.47	1.2×10^{22}	2.1	2.00×10^{21}	1.9	1.0	0.6	40%	(Fukuda et al., 2012)
W-3%*Re*	neutron	873	0.15	1.40×10^{22}	3.6	3.40×10^{22}	1.1	0.7	1.0	43%	(He et al., 2006)
W-3%*Re*	neutron	1073	0.15	1.10×10^{22}	2.8	9.00×10^{21}	1.3	0.6	0.7	17%	(He et al., 2006)
W-5%*Re*	neutron	804	0.44	1.40×10^{22}	2.9	2.00×10^{21}	1.7	0.8	0.8	0%	(Fukuda et al., 2012)
W-5%*Re*	neutron	856	0.47	1.3×10^{22}	2.2	3.00×10^{21}	1.6	1.1	0.7	36%	(Fukuda et al., 2012)
W-10% *Re*	neutron	804	0.44	3.0×10^{21}	7.1	1.00×10^{21}	3.4	1.0	0.6	40%	(Fukuda et al., 2012)
W-10% *Re*	neutron	856	0.47	6.0×10^{21}	4.5	5.00×10^{20}	3.9	1.1	0.7	36%	(Fukuda et al., 2012)

Here the helium bubble spacing L in τ_H is $1/\sqrt{ND}$, where N are D the density and diameter of helium bubbles, respectively.

When predicting helium bubble hardening, the proportional model of screw and edge dislocations established in Section 6.1.2 can be used. One can also simplify the prediction by considering the difference of the dominant dislocations in BCC tungsten at different temperatures as follows. Firstly, a critical temperature T_c is defined according to the ratio of screw dislocation velocity to edge dislocation velocity. T_c is set as 800 K here for tungsten according to Fig. 17(b), beyond which the screw dislocation velocity rises to a non-negligible degree. It means the edge dislocation density increases and plastic deformation transform from screw dislocation

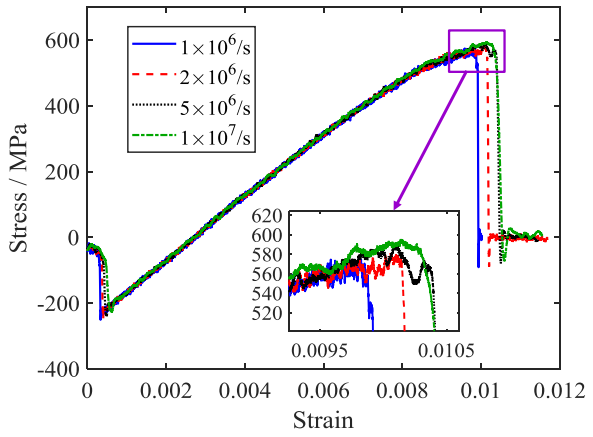

Fig. A1. Stress-strain curves of a straight edge dislocation interacting with a 5 nm void simulated by strain rate 1×10^6/s, 2×10^6/s, 5×10^6/s and 1×10^7/s, respectively.

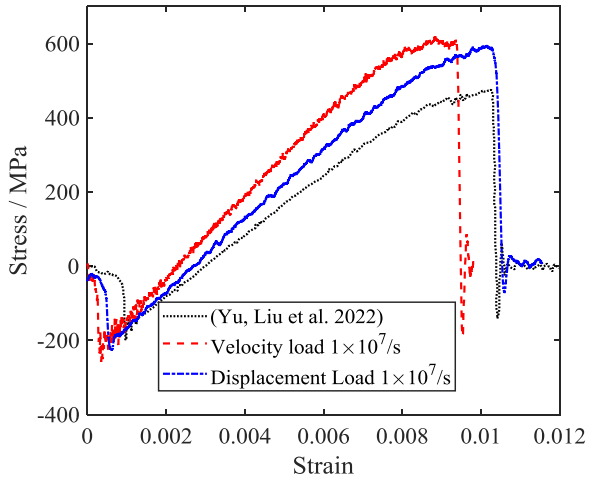

Fig. A2. Stress-strain curve of a straight edge dislocation interacting with a 5 nm void from literature (Yu et al., 2022), velocity load simulation of applied strain rate $1 \times 10^7/s$, displacement load of strain rate $1 \times 10^7/s$.

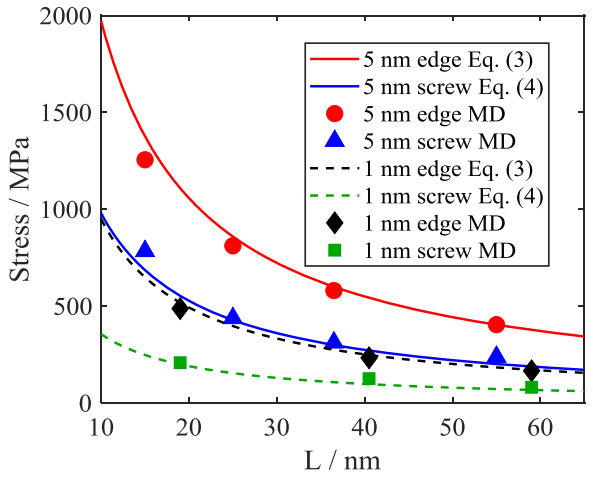

Fig. B1. Comparation of hardening stress of edge and screw dislocation interacting with a 5 nm or 1 nm helium bubble with He/$V = 2$ from hardening model prediction and MD simulation.

dominated to edge or edge-like dislocation dominated as temperature reaches T_c. When the temperature is lower than the critical temperature T_c, it can be simply considered that all the dislocations in tungsten are screw, and when the temperature is higher than T_c, all of them are edge or similar to edge dislocations for its mobility behavior. For $T< T_c$, the hardening model for interaction between helium bubbles and screw dislocations expressed as Eq. (4) is used here, and for elevated temperatures that for edge dislocations expressed as Eq. (3) is used.

The comparison between the predicted and experimental results is shown in Table 1. The predicted hardness increment are close to those from experiments for all these available cases, which further demonstrates the reliability of the developed model.

7. Summary and conclusions

Helium bubbles produced in fusion reactor environments strongly impact the performance of plasma-facing components. However, the interaction between helium bubbles and dislocations is a complex physical process, which is influenced by the external temperature, and the internal features of dislocations and helium bubbles, such as dislocation type, helium bubble size and the He/V ratio etc. Till now, there is lack of systematic studies disclosing the interaction mechanism between dislocation and helium bubble. Therefore, it is highly required to propose quantitative theoretical and numerical models.

This work reveals the interaction mechanism between dislocations and helium bubbles in tungsten, establishes the mechanism phase diagrams in the space of helium bubble size and He/V ratio, and proposes the atomistic mechanism-based helium bubble kinetics and hardening models. The established model can be directly applied to multiscale simulations, such as DDD and CP, providing a bridge between atomic-scale insights and micro-scale behaviors. Additionally, the proposed hardening model well predicts the irradiation hardening behavior in the available macroscopic experiments at different temperatures. In addition, the following conclusions are gained.

The equilibrium He/V ratio of helium bubble varies with the material property and irradiation environment. When He/V ratio is higher than the equilibrium ratio, helium bubble is mechanically unstable, and interaction between dislocations and helium bubbles is the over-pressured bubble dominated. On the other hand, in the stable range of He/V ratio, the He/V ratio has little effect on the interaction mechanism and mechanical response.

Increasing helium bubble size will lead to the transition from shear to Orowan-like or cross slip mechanism for the interaction between helium bubble and edge or screw dislocation, respectively. In the Orowan-like mechanism region, depinning of edge dislocation is climb assisted, while depinning is cross slip assisted for screw dislocation.

Mechanism-based reaction kinetics model for helium bubble is proposed. When the helium bubble size is less than 5 nm, the geometry of climbed edge dislocation after the interaction shows self-similarity. Based on this insight, the size variation of the helium bubble after interacting with edge dislocation is found to satisfy the uniform quadratic function relationship. On the other hand, interaction of the screw dislocation with the helium bubble does not change the size of the helium bubble.

The characteristic length of helium bubbles interacting with different types of dislocations is revealed, and a unified helium bubble hardening model applicable to edge, screw and mixed dislocations is established. Additionally, a yield strength model for irradiated tungsten is developed, which considers the temperature dependent plasticity of BCC materials, and the temperature independent irradiation hardening of helium bubbles. The predicted results of the model are in good agreement with the simulation results of MD for various dislocation types and helium bubble sizes, as well as the macroscopic experimental results.

Author statement

CQ Ji: Investigation, Methodology, Formal analysis, Writing - original draft; **JQ Hu:** Discussion, Verification, Writing - review & editing; **Z Zhuang:** Discussion, Supervision, Writing - review & editing; **YN Cui:** Conceptualization, Supervision, Methodology, Formal analysis, Writing - original draft, Writing - review & editing

Declaration of Competing Interest

The authors declare that they have no known competing financial interests or personal relationships that could have appeared to influence the work reported in this paper.

Data availability

Data will be made available on request.

Acknowledgement

This material is based upon work supported by the National Natural Science Foundation of China under Grant No. 12172194, 12222205, 11972208, 11921002, and Key R&D projects of the Ministry of Science and Technology 2022YFB4603000.

Appendix A

Verification of molecular dynamics models

The MD model built in Section 2 is verified in this section by checking the influence of simulation box size and strain rate, and comparing simulation results with existing literature.

Firstly, for the effect of simulation box size, the lengths of simulation box in x (dislocation glide direction) and y (normal direction of slip plane) directions used in this study are expanded to about 1.5 times their initial value to study the interaction of an edge dislocation and a 5 nm void, respectively. It shows that changes of CRSS before and after modifying the simulation size are within 1.5%, indicating the value of L_x and L_y chosen in this study is reasonable.

Secondly, in order to test the strain rate effect, the stress-strain curves of edge dislocation-void interaction in displacement load under strain rates of 1×10^6/s, 2×10^6/s, 5×10^6/s and 1×10^7/s are compared in Fig. A1. It is clear that the difference in stress-strain curve gained from strain rates above is small compared to the value of CRSS, which implies that the strain rate of 1×10^7/s used in this study is reasonable.

Furthermore, the shear modulus of the perfect tungsten single crystal at 300 K from simulation is 181.8 GPa, which is close to the results of 178 GPa in previous work (Osetsky, 2021). The calculated result of edge dislocation interacting with a 5 nm void at 300 K is compared with the existing literature (Yu et al., 2022), as shown in Fig. A2. It is found that the hardening stress was close to the previous work and within the allowable range of molecular dynamics simulation. Besides displacement loading used in this study, velocity loading mode, in which flexible boundary condition is used in the upper and lower layer to reduce stress oscillation (Jian et al., 2020), is also simulated, and its results are basically consistent with that from displacement loading, which further illustrates the effectiveness of the model.

Appendix B

Influence of helium bubble spacing on hardening

According to the helium bubble hardening model expressed as Eq. (3) and (4), helium bubble spacing L has a significant effect on hardening stress. To verify the effectiveness of proposed unfiled hardening model, interaction of 1 nm and 5 nm helium bubbles with edge and screw dislocations with different L are calculated. As shown in Fig. B1, simulation results are in good agreement with the predicted data by proposed hardening model under the wide range of helium bubble spacings we studied, indicating the reliability of the proposed hardening model.

References

Bacon, D.J., Kocks, U.F., Scattergood, R.O., 1973. The effect of dislocation self-interaction on the orowan stress. Philos. Mag. 28 (6), 1241–1263.

Bacon, D.J., Osetsky, Y.N., 2005. Modelling dislocation–obstacle interactions in metals exposed to an irradiation environment. Mater. Sci. Eng. 400-401, 353–361.

Beck, C.E., Hofmann, F., Eliason, J.K., Maznev, A.A., Nelson, K.A., Armstrong, D.E.J., 2017. Correcting for contact area changes in nanoindentation using surface acoustic waves. Scr. Mater. 128, 83–86.

Boisse, J., Domain, C., Becquart, C.S., 2014. Modelling self trapping and trap mutation in tungsten using DFT and Molecular Dynamics with an empirical potential based on DFT. J. Nucl. Mater. 455 (1–3), 10–15.

Bonny, G., Grigorev, P., Terentyev, D., 2014. On the binding of nanometric hydrogen-helium clusters in tungsten. J. Phys. 26 (48), 485001.

Brunner, D., 2010. Temperature dependence of the plastic flow of high-purity tungsten single crystals. Int. J. Mater. Res. 8, 101.

Butler, B.G., Paramore, J.D., Ligda, J.P., Ren, C., Fang, Z.Z., Middlemas, S.C., Hemker, K.J., 2018. Mechanisms of deformation and ductility in tungsten – a review. Int. J. Refractory Metals Hard Mater. 75, 248–261.

Chen, W.Q., Wang, X.Y., Xiao, X.Z., Qu, S.L., Jia, Y.Z., Cui, W., Cao, X.Z., Xu, B., Liu, W., 2018. Characterization of dose dependent mechanical properties in helium implanted tungsten. J. Nucl. Mater. 509, 260–266.

Chen, Z.M., Mrovec, M., Gumbsch, P., 2011. Dislocation–vacancy interactions in tungsten. Model. Simul. Mater. Sci. Eng. 19 (7), 074002.

Cui, J., Li, M., Wang, J., Hou, Q., 2015. Molecular dynamics study of helium bubble pressure in tungsten. Nucl. Instrum. Methods Phys. Res. Sect. B 352, 104–106.

Cui, W., Cui, Y., Liu, W., 2021a. A statistical model of irradiation hardening induced by non-periodic irradiation defects. Scr. Mater. 201, 113959.

Cui, Y., Ghoniem, N., Po, G., 2021b. Plasticity of irradiated materials at the nano and micro-scales. J. Nucl. Mater. 546, 152746.

Cui, Y., Po, G., Ghoniem, N., 2016. Temperature insensitivity of the flow stress in body-centered cubic micropillar crystals. Acta Mater. 108, 128–137.

Cui, Y., Po, G., Ghoniem, N., 2017. Does irradiation enhance or inhibit strain bursts at the submicron scale? Acta Mater. 132, 285–297.

Cui, Y., Po, G., Ghoniem, N., 2018a. Size-tuned plastic flow localization in irradiated materials at the submicron scale. Phys. Rev. Lett. 120 (21), 215501.

Cui, Y., Po, G., Ghoniem, N.M., 2018b. A coupled dislocation dynamics-continuum barrier field model with application to irradiated materials. Int. J. Plasticity 104, 54–67.

Das, S., Armstrong, D.E.J., Zayachuk, Y., Liu, W., Xu, R., Hofmann, F., 2018. The effect of helium implantation on the deformation behaviour of tungsten: x-ray micro-diffraction and nanoindentation. Scr. Mater. 146, 335–339.

Das, S., Yu, H., Mizohata, K., Tarleton, E., Hofmann, F., 2020. Modified deformation behaviour of self-ion irradiated tungsten: a combined nano-indentation, HR-EBSD and crystal plasticity study. Int. J. Plasticity 135, 102817.

Das, S., Yu, H., Tarleton, E., Hofmann, F., 2019. Hardening and strain localisation in helium-ion-implanted tungsten. Sci. Rep. 9 (1), 18354.

Daw, M.S., Baskes, M.I., 1984. Embedded-atom method: derivation and application to impurities, surfaces, and other defects in metals. Phys. Rev. B 29 (12), 6443–6453.

Ding, M.S., Tian, L., Han, W.Z., Li, J., Ma, E., Shan, Z.W., 2016. Nanobubble fragmentation and bubble-free-channel shear localization in helium-irradiated submicron-sized copper. Phys. Rev. Lett. 117 (21), 215501.

Dong, W., Liu, H., Du, J., Zhang, X., Huang, M., Li, Z., Chen, Z., Bobaru, F., 2022. A peridynamic approach to solving general discrete dislocation dynamics problems in plasticity and fracture: part I. Model description and verification. Int. J. Plasticity 157, 103401.

Dutta, A., Bhattacharya, M., Gayathri, N., Das, G.C., Barat, P., 2012. The mechanism of climb in dislocation–nanovoid interaction. Acta Mater. 60 (9), 3789–3798.

Faney, T., 2013. Numerical Simulations of Tungsten under Helium Irradiation. PhD thesis. University of California.

Fukuda, M., Kiran Kumar, N.A.P., Koyanagi, T., Garrison, L.M., Snead, L.L., Katoh, Y., Hasegawa, A., 2016. Neutron energy spectrum influence on irradiation hardening and microstructural development of tungsten. J. Nucl. Mater. 479, 249–254.
Fukuda, M., Tanno, T., Nogami, S., Hasegawa, A., 2012. Effects of *Re* content and fabrication process on microstructural changes and hardening in neutron irradiated tungsten. Mater. Trans. 53 (12), 2145–2150.
Gao, E., Ghoniem, N.M., 2018. A coupled rate theory-Monte Carlo model of helium bubble evolution in plasma-facing micro-engineered tungsten. J. Nucl. Mater. 509, 577–590.
Ghoniem, N.M., Cui, Y., 2020. Dislocation dynamics simulations of defects in irradiated materials. Compr. Nucl. Mater. 689–716.
Grammatikopoulos, P., Bacon, D.J., Osetsky, Y.N., 2011. The influence of interaction geometry on the obstacle strength of voids and copper precipitates in iron. Model. Simul. Mater. Sci. Eng. 19 (1), 015004.
Grigorev, P., Zinovev, A., Terentyev, D., Bonny, G., Zhurkin, E.E., Van Oost, G., Noterdaeme, J.-M., 2018. Molecular dynamics simulation of hydrogen and helium trapping in tungsten. J. Nucl. Mater. 508, 451–458.
Guo, X., Sun, C., Wang, C., Jiang, J., Fu, M.W., 2021. Study of dislocation-twin boundary interaction mechanisms in plastic deformation of TWIP steel by discrete dislocation dynamics and dislocation density-based modeling. Int. J. Plasticity 145, 103076.
Hafez Haghighat, S.M., Schaeublin, R., 2008. Molecular dynamics modeling of cavity strengthening in irradiated iron. J. Comput.-Aided Mater. Des. 14 (S1), 191–201.
Hafez Haghighat, S.M., Schäublin, R., 2010. Influence of the stress field due to pressurized nanometric He bubbles on the mobility of an edge dislocation in iron. Philos. Mag. 90 (7–8), 1075–1100.
Hamid, A.Y., Sun, J., Zhang, H., Jadon, A.S., Stirner, T., 2019. Molecular dynamics simulations of helium clustering and bubble growth under tungsten surfaces. Comput. Mater. Sci. 163, 141–147.
Hammond, K.D., Blondel, S., Hu, L., Maroudas, D., Wirth, B.D., 2018. Large-scale atomistic simulations of low-energy helium implantation into tungsten single crystals. Acta Mater. 144, 561–578.
Harrison, R.W., Greaves, G., Hinks, J.A., Donnelly, S.E., 2017. Engineering self-organising helium bubble lattices in tungsten. Sci. Rep. 7 (1), 7724.
He, J.C., Tang, G.Y., Hasegawa, A., Abe, K., 2006. Microstructural development and irradiation hardening of W and W–(3–26) wt%*Re* alloys after high-temperature neutron irradiation to 0.15 dpa. Nucl. Fus. 46 (11), 877–883.
Hirai, T., Escourbiac, F., Carpentier-Chouchana, S., Durocher, A., Fedosov, A., Ferrand, L., Jokinen, T., Komarov, V., Merola, M., Mitteau, R., Pitts, R.A., Shu, W., Sugihara, M., Barabash, V., Kuznetsov, V., Riccardi, B., Suzuki, S., 2014. ITER full tungsten divertor qualification program and progress. Physica Scripta T159, 014006.
Hirel, P., 2015. Atomsk: a tool for manipulating and converting atomic data files. Comput. Phys. Commun. 197, 212–219.
Hu, X., Koyanagi, T., Fukuda, M., Kumar, N.A.P.K., Snead, L.L., Wirth, B.D., Katoh, Y., 2016. Irradiation hardening of pure tungsten exposed to neutron irradiation. J. Nucl. Mater. 480, 235–243.
Huang, X., Lv, C., Chu, H., 2021. Anomalous shape effect of nanosized helium bubble on the elastic field in irradiated tungsten. Sci. Rep. 11 (1), 830.
Ipatova, I., Greaves, G., Pacheco-Gutiérrez, S., Middleburgh, S.C., Rushton, M.J.D., Jimenez-Melero, E., 2021. In-situ TEM investigation of nano-scale helium bubble evolution in tantalum-doped tungsten at 800°C. J. Nucl. Mater. 550, 152910.
Ito, A.M., Yoshimoto, Y., Saito, S., Takayama, A., Nakamura, H., 2014. Molecular dynamics simulation of a helium bubble bursting on tungsten surfaces. Physica Scripta T159, 014062.
Ji, C., Cui, Y., Li, Y., Ghoniem, N., 2022. A concurrent irradiation-mechanics multiscale coupling model. J. Mech. Phys. Solids 167, 105005.
Jian, W.-R., Zhang, M., Xu, S., Beyerlein, I.J., 2020. Atomistic simulations of dynamics of an edge dislocation and its interaction with a void in copper: a comparative study. Model. Simul. Mater. Sci. Eng. 28 (4), 045004.
Kong, F., Qu, M., Yan, S., Zhang, A., Peng, S., Xue, J., Wang, Y., 2017. Helium-induced hardening effect in polycrystalline tungsten. Nucl. Instrum. Methods Phys. Res. Sect. B 406, 643–647.
Koyanagi, T., Kumar, N.A.P.K., Hwang, T., Garrison, L.M., Hu, X., Snead, L.L., Katoh, Y., 2017. Microstructural evolution of pure tungsten neutron irradiated with a mixed energy spectrum. J. Nucl. Mater. 490, 66–74.
Li, B., Jin, S., Xu, K., Hao, J., Shu, X., 2019. Atomistic simulations of the interactions between the 1/2 ⟨1 1 1⟩ {1 1 0} edge dislocations and the intrinsic point defects in tungsten. Nucl. Instrum. Methods Phys. Res. Sect. B 459, 59–63.
Li, X.-C., Liu, Y.-N., Yu, Y., Luo, G.-N., Shu, X., Lu, G.-H., 2014. Helium defects interactions and mechanism of helium bubble growth in tungsten: a molecular dynamics simulation. J. Nucl. Mater. 451 (1–3), 356–360.
Li, Z., Liu, Z., Zhuang, Z., Cui, Y., 2021. Temperature dependent deformation localization in irradiated tungsten. Int. J. Plasticity 146, 103077.
Liu, W., Chen, L., Yu, L., Fu, J., Duan, H., 2022. Continuum modeling of dislocation channels in irradiated metals based on stochastic crystal plasticity. Int. J. Plasticity 151, 103211.
Liu, X.L., Golubov, S.I., Woo, C.H., Huang, H.C., 2004. Atomistic simulations of dislocation-void interactions using green's function boundary relaxation. Comput. Model. Eng. Sci. 5 (6), 527–539.
Lu, S., Zhao, J., Huang, M., Li, Z., Kang, G., Zhang, X., 2022. Multiscale discrete dislocation dynamics study of gradient nano-grained materials. Int. J. Plasticity 156, 103356.
Lu, Y., Zhang, Y.H., Ma, E., Han, W.Z., 2021. Relative mobility of screw versus edge dislocations controls the ductile-to-brittle transition in metals. Proc. Natl. Acad. Sci. U.S.A. 118 (37).
Marinica, M.C., Ventelon, L., Gilbert, M.R., Proville, L., Dudarev, S.L., Marian, J., Bencteux, G., Willaime, F., 2013. Interatomic potentials for modelling radiation defects and dislocations in tungsten. J. Phys. 25 (39), 395502.
Nishijima, D., Ye, M.Y., Ohno, N., Takamura, S., 2004. Formation mechanism of bubbles and holes on tungsten surface with low-energy and high-flux helium plasma irradiation in NAGDIS-II. J. Nucl. Mater. 329-333, 1029–1033.
Osetsky, Y.N., 2021. Atomic-scale mechanisms of void strengthening in tungsten. Tungsten 3 (1), 65–71.
Osetsky, Y.N., Bacon, D.J., 2003a. An atomic-level model for studying the dynamics of edge dislocations in metals. Model. Simul. Mater. Sci. Eng. 11, 427.
Osetsky, Y.N., Bacon, D.J., 2003b. Void and precipitate strengthening in α-iron: what can we learn from atomic-level modelling? J. Nucl. Mater. 323 (2–3), 268–280.
Osetsky, Y.N., Bacon, D.J., 2010. Atomic-scale mechanisms of void hardening in bcc and fcc metals. Philos. Mag. 90 (7–8), 945–961.
Osetsky, Y.N., Bacon, D.J., Mohles, V., 2003. Atomic modelling of strengthening mechanisms due to voids and copper precipitates in α-iron. Philos. Mag. 83 (31–34), 3623–3641.
Osetsky, Y.N., Stoller, R.E., 2015. Atomic-scale mechanisms of helium bubble hardening in iron. J. Nucl. Mater. 465, 448–454.
Pavlina, E.J., Van Tyne, C.J., 2008. Correlation of yield strength and tensile strength with hardness for steels. J. Mater. Eng. Perform. 17 (6), 888–893.
Plimpton, S., 1995. Fast parallel algorithms for short-range molecular dynamics. J. Comput. Phys. 117, 1–19.
Po, G., Cui, Y., Rivera, D., Cereceda, D., Swinburne, T.D., Marian, J., Ghoniem, N., 2016. A phenomenological dislocation mobility law for bcc metals. Acta Mater. 119, 123–135.
Rigelesaiyin, J., Diaz, A., Li, W., Xiong, L., Chen, Y., 2018. Asymmetry of the atomic-level stress tensor in homogeneous and inhomogeneous materials. Proc. 474 (2217), 20180155.
Rodney, D., 2004. Molecular dynamics simulation of screw dislocations interacting with interstitial frank loops in a model FCC crystal. Acta Mater. 52, 607–614.
Russell, K.C., Brown, L.M., 1972. Dispersion strengthening model based on differing elastic-moduli applied to iron-copper system. Acta Metallurgica 20, 969–974.
Scattergood, R.O., Bacon, D.J., 1982. The strengthening effect of voids. Acta Metallurgica 30 (8), 1665–1677.
Shi, J., Liu, G., Wu, K., Yu, P., Zhu, H., Zhao, G., Shen, Y., 2022. Experiments and/or crystal plasticity finite element modeling of the mechanical properties of pristine and irradiated tungsten single crystal. Int. J. Plasticity 154, 103293.
Sobie, C., Bertin, N., Capolungo, L., 2015. Analysis of obstacle hardening models using dislocation dynamics: application to irradiation-induced defects. Metal. Mater. Trans. A 46 (8), 3761–3772.
Stukowski, A., 2010. Visualization and analysis of atomistic simulation data with OVITO–the open visualization tool. Model. Simul. Mater. Sci. Eng. 18 (1), 015012.

Tehranchi, A., Zhang, X., Lu, G., Curtin, W.A., 2017. Hydrogen–vacancy–dislocation interactions in α-Fe. Model. Simul. Mater. Sci. Eng. 25 (2), 025001.
Terentyev, D., Bacon, D.J., Osetsky, Y.N., 2008. Interaction of an edge dislocation with voids in α-iron modelled with different interatomic potentials. J. Phys. 20 (44), 445007.
Tian, X., Woo, C., 2004. The movement of screw dislocations in tungsten. Mater. Sci. Eng. 369 (1–2), 210–214.
Tougou, K., Fukui, M., Fukumoto, K.-I., Ishigami, R., Yabuuchi, K., 2022. Dynamic interaction between the dislocations and cavities in tungsten during tensile test. Nucl. Mater. Energy 30, 101130.
Trinkaus, H., Singh, B.N., 2003. Helium accumulation in metals during irradiation – where do we stand? J. Nucl. Mater. 323 (2–3), 229–242.
Vítek, V., Perrin, R.C., Bowen, D.K., 1970. The core structure of ½(111) screw dislocations in b.c.c. crystals. Philos. Mag. 21 (173), 1049–1073.
Wang, J., Liu, D., Dang, W., Guo, Z., Song, W., 2021a. Segregation and coalescence behavior of helium bubbles in tungsten. J. Nucl. Mater. 544, 152732.
Wang, J., Liu, D., Guo, Z., He, B., Dang, W., 2021b. Molecular dynamics study on the origin of fuzz structure on tungsten surface. J. Nucl. Mater.. 547, 152835.
Wang, J., Niu, L.-L., Shu, X., Zhang, Y., 2015. Energetics and kinetics unveiled on helium cluster growth in tungsten. Nucl. Fus. 55 (9), 092003.
Wang, Q., Cochrane, C., Skippon, T., Wang, Z., Abdolvand, H., Daymond, M.R., 2020. Orientation-dependent irradiation hardening in pure Zr studied by nanoindentation, electron microscopies, and crystal plasticity finite element modeling. Int. J. Plasticity 124, 133–154.
Weaver, J.S., Sun, C., Wang, Y., Kalidindi, S.R., Doerner, R.P., Mara, N.A., Pathak, S., 2017. Quantifying the mechanical effects of He, W and He + W ion irradiation on tungsten with spherical nanoindentation. J. Mater. Sci. 53 (7), 5296–5316.
Wen, W., Kohnert, A., Arul Kumar, M., Capolungo, L., Tomé, C.N., 2020. Mechanism-based modeling of thermal and irradiation creep behavior: an application to ferritic/martensitic HT9 steel. Int. J. Plasticity 126, 102633.
Wolfer, W.G., 1988. The pressure for dislocation loop punching by a single bubble. Philos. Mag. A 58 (2), 285–297.
Xie, H., Xu, K., Lu, G.-H., Yu, T., Yin, F., 2018. Dislocation climbing mechanism for helium bubble growth in tungsten. Scr. Mater. 147, 98–102.
Xu, S., McDowell, D.L., Beyerlein, I.J., 2019. Sequential obstacle interactions with dislocations in a planar array. Acta Mater. 174, 160–172.
Yan, J., 2006. Strength Modelling of Al-Cu-Mg Type Alloys. PhD thesis. University of Southampton.
Ye, M., Zhan, J., Mao, S., Liu, Z., Ding, Y., 2020. Simulation study of evolution of helium induced defects in bulk tungsten. Fus. Eng. Des. 158, 111864.
Yi, X., Arakawa, K., Nguyen-Manh, D., Ferroni, F., Liu, P., Han, W., Wan, F., Roberts, S.G., 2017. A study of helium bubble production in 10keV He+ irradiated tungsten. Fus. Eng. Des. 125, 454–457.
Yu, P., Liu, G., Wu, K., Cui, Y., Zhao, G., Shen, Y., 2022. Exploring the effects of the sheared voids on the hardening of tungsten using atomistic simulations. J. Nucl. Mater. 562, 153548.
Zhan, J., Ye, M., Mao, S., Ren, J., Xu, X., 2019. Simulation study of evolution of helium bubbles in bulk tungsten. Fus. Eng. Des. 146, 983–986.
Zhang, H., Sun, J., Wang, Y., Qin, M., Stirner, T., 2022. Molecular dynamics simulation analysis of the stress around an up-migrating helium bubble under tungsten surface and its bursting. Mater. Today Commun. 31, 103602.
Zhang, H., Sun, J., Wang, Y., Stirner, T., Hamid, A.Y., Sang, C., 2020. Study of lattice thermal conductivity of tungsten containing bubbles by molecular dynamics simulation. Fus. Eng. Des. 161, 112004.
Zhang, P., Li, S.X., Zhang, Z.F., 2011. General relationship between strength and hardness. Mater. Sci. Eng. 529, 62–73.
Zinkle, S.J., Busby, J.T., 2009. Structural materials for fission & fusion energy. Mater. Today 12 (11), 12–19.